



## Targeted liposomal doxorubicin/ceramides combinations: The importance to assess the nature of drug interaction beyond bulk tumor cells

Ana Filipa Cruz<sup>a,b</sup>, Nuno A. Fonseca<sup>a,c</sup>, Ana Rita Malheiro<sup>d,e</sup>, Joana B. Melo<sup>f,g</sup>,  
 Maria Manuela Gaspar<sup>h</sup>, Rui Fernandes<sup>d,e</sup>, Vera Moura<sup>a,c</sup>, Sérgio Simões<sup>a,b</sup>,  
 João Nuno Moreira<sup>a,b,\*</sup>

<sup>a</sup> CNC – Center for Neurosciences and Cell Biology, Center for Innovative Biomedicine and Biotechnology (CIBB), University of Coimbra, Faculty of Medicine (Polo 1), Rua Larga, 3004-504 Coimbra, Portugal

<sup>b</sup> Univ Coimbra - University of Coimbra, CIBB, Faculty of Pharmacy, Pólo das Ciências da Saúde, Azinhaga de Santa Comba, 3000-548 Coimbra, Portugal

<sup>c</sup> TREAT U, SA - Parque Industrial de Taveiro, Lote 44, 3045-508 Coimbra, Portugal

<sup>d</sup> HEMS—Histology and Electron Microscopy, i3S-Instituto de Investigação e Inovação em Saúde, University of Porto, 4200-135 Porto, Portugal

<sup>e</sup> IBMC—Instituto de Biologia Molecular e Celular, University of Porto, 4200-135 Porto, Portugal

<sup>f</sup> iCBR—Coimbra Institute for Clinical and Biomedical Research, CIBB, Center of Investigation on Environment Genetics and Oncobiology (CIMAGO), Pólo das Ciências da Saúde, Azinhaga de Santa Comba, 3000-548 Coimbra, Portugal

<sup>g</sup> Univ Coimbra—University of Coimbra, Clinical Academic Center of Coimbra (CACC), Faculty of Medicine, Pólo das Ciências da Saúde, Azinhaga de Santa Comba, 3000-548 Coimbra, Portugal

<sup>h</sup> iMed.Ulissboa, Research Institute for Medicines – Faculty of Pharmacy, University of Lisbon, Av. Prof. Gama Pinto, 1649-003 Lisboa, Portugal

### ARTICLE INFO

#### Keywords:

Triple-negative breast cancer  
 Doxorubicin  
 C6-ceramide  
 C18-ceramide  
 Nature of drug interaction  
 Synergistic combinations  
 Cancer stem cells

### ABSTRACT

One of the major assets of anticancer nanomedicine is the ability to co-deliver drug combinations, as it enables targeting of different cellular populations and/or signaling pathways implicated in tumorigenesis and thus tackling tumor heterogeneity. Moreover, drug resistance can be circumvented, for example, upon co-encapsulation and delivery of doxorubicin and sphingolipids, as ceramides. Herein, the impact of short (C6) and long (C18) alkyl chain length ceramides on the nature of drug interaction, within the scope of combination with doxorubicin, was performed in bulk triple-negative breast cancer (TNBC) cells, as well as on the density of putative cancer stem cells and phenotype, including live single-cell tracking.

C6- or C18-ceramide enabled a synergistic drug interaction in all conditions and (bulk) cell lines tested. However, differentiation among these two ceramides was reflected on the migratory potential of cancer cells, particularly significant against the highly motile MDA-MB-231 cells. This effect was supported by the down-regulation of the PI3K/Akt pathway enabled by C6-ceramide and in contrast with C18-ceramide. The decrease of the migratory potential enabled by the targeted liposomal combinations is of high relevance in the context of TNBC, due to the underlying metastatic potential.

Surprisingly, the nature of the drug interaction assessed at the level of bulk cancer cells revealed to be insufficient to predict whether a drug combination enables a decrease in the percentage of the master regulators of tumor relapse as ALDH<sup>+/high</sup> putative TNBC cancer stem cells, suggesting, for the first time, that it should be extended further down to this level.

### 1. Introduction

Triple-negative breast cancer (TNBC) is characterized by the absence of the expression of estrogen and progesterone receptors and the human epidermal growth factor receptor 2 (HER2). This lack of well-defined molecular markers limits the current first line systemic therapeutic

options to conventional anticancer drugs, as doxorubicin (DXR), incorporated in some protocols [1–3]. However, these drugs have local and systemic toxicity, such as DXR-induced cardiotoxicity, resulting from the lack of tissue/cell specificity which ultimately could lead to treatment failure [4]. Moreover, a population of cancer cells, named as cancer stem cells (CSCs), has been described to be resistant to

\* Corresponding author.

E-mail address: [jmoreira@ff.uc.pt](mailto:jmoreira@ff.uc.pt) (J.N. Moreira).

<https://doi.org/10.1016/j.ejpb.2022.01.006>

Received 14 September 2021; Received in revised form 14 January 2022; Accepted 18 January 2022

Available online 31 January 2022

0939-6411/© 2022 Elsevier B.V. All rights reserved.

conventional chemotherapy due to intrinsic or acquired mechanisms, such as superior DNA-repair capacity or upregulation of drug-efflux pumps (for example, ATP-binding cassette transporters such as P-glycoprotein), thus increasing the probability of tumor relapse [5,6]. Furthermore, the plasticity associated with CSCs and non-stem cancer cells, which interconvert according to environmental stimuli, illustrates the cellular dynamics within the tumor microenvironment and contributes to drug resistance and tumor progression [5,7]. Specifically, the progression to a metastatic disease has been associated to epithelial-to-mesenchymal transition, a biological process that confers a mesenchymal phenotype, allowing tumor cells with a cancer stem phenotype to disseminate [7,8]. It is thus important to properly identify this critical sub-population of cells, with an overall impact on tumorigenicity.

Surface markers, such as CD44 and CD24, and functional markers, such as aldehyde dehydrogenase (ALDH) activity, have been used to identify putative CSC population in breast cancer [9–11]. Sphere-forming assays, an *in vitro* functional assay, have also been reported as an indicator of the enhanced self-renewal at the single-cell level [12]. Of relevance in the functional establishment of CSCs are, as a complement, the (*in vivo*) tumorigenic assays [13–15]. Additionally, overexpression of the regulatory transcription factors OCT4 and NANOG has been described as a central regulator of CSCs self-renewal and has been associated with poor prognosis in breast cancer patients [16–18].

The acknowledgment that simultaneous targeting of different tumor cell populations could increase efficacy of new anticancer therapeutic strategies [19], led to the need to identify common markers among those. In this respect, nucleolin overexpression has been demonstrated on the cell surface of breast CSCs, non-stem breast cancer cells and endothelial cells from the tumor blood vessels, emerging as a potential common marker for different breast tumor cell populations [20–22].

Nucleolin can be identified in several cellular compartments, being predominantly located in the nucleolus. It is involved in chromatin structure, regulation of transcription, ribosome assembly and nucleus-cytoplasm transport [23,24]. While surface nucleolin has been described as a target for several ligands, some of them implicated in carcinogenesis, such as pleiotrophin and P-selectin [25], it has also become a relevant marker for anticancer therapies and some nucleolin-binding ligands have been generated, such as the antagonistic pseudo-peptides HB-19 and N6L [26,27], the aptamer AS1411 [28] or the F3 peptide [29].

A nucleolin-binding F3 peptide-targeted pegylated and pH-sensitive lipid nanoparticle was developed to co-encapsulate a combination of DXR and C6- or C18-ceramide, at a 1:1 molar ratio. The former, a well-known topoisomerase II inhibitor, induces dose-dependent cytotoxicity in non-stem cancer cells [30,31] and has been described to induce the accumulation of endogenous ceramides, a critical component of the apoptosis signaling cascade [32], further enhancing the cytotoxic effects. However, the overexpression of glucosylceramide synthase, an enzyme described to metabolize ceramides [33], has been associated with the development of resistance to DXR by reducing the cytotoxicity induced by ceramides [34,35]. Therefore, co-administration of exogenous ceramides and DXR has been demonstrated to be a useful strategy to enhance antitumor effects against several types of cancer [36–38]. In addition, intracellular delivery of DXR encapsulated in lipid nanoparticles has the additional advantage to partially circumvent P-glycoprotein-mediated drug resistance [39].

C6-ceramide is a short-chain sphingolipid associated with rapid transbilayer movements, being able to dissociate from the liposomal phospholipid bilayer [40,41] whereas a long-chain sphingolipid, as C18-ceramide, has been associated with enhanced stability within the liposomal membrane [36]. Both ceramides are pro-apoptotic sphingolipids [42–44] and C6-ceramide has been demonstrated to downregulate the PI3K/Akt pathway [45,46], often described as being overexpressed in CSCs [42,47–49]. Furthermore, *in vivo* studies showed that intravenous administration of liposomal C6-ceramide was well tolerated by female BALB/c mice and inhibited tumor growth of a syngeneic mouse solid

tumor model of mammary adenocarcinoma [50] and human hepatocellular carcinoma xenografts in athymic nude mice relative to untreated control and liposomes without C6-ceramide [51].

Accordingly, the aim of the present work is to determine the nature of the interaction between nucleolin-targeted liposomal combinations of DXR and ceramides with different alkyl chain lengths in TNBC cell lines and assess for the first time, to the best of the authors knowledge, how this effect, determined at the level of bulk cells, impacts the viability of a master cell regulator of tumor aggressiveness as putative triple-negative breast CSC population. The effect of the alkyl chain length within the scope of the referred drug combinations was further evaluated on the mRNA levels of pluripotency transcription factors and on the phenotype of TNBC cells, including mammosphere forming efficiency and live single-cell tracking.

## 2. Materials and methods

### 2.1. Materials

Doxorubicin hydrochloride was provided by MicroBiopharm (Japan). 4-(2-hydroxyethyl)piperazine-1-ethanesulfonic acid (HEPES), Disodium ethylenediaminetetraacetate dehydrate (EDTA), resazurin, sephadex G-50, ammonium sulphate, sodium chloride, 3 $\beta$ -hydroxy-5-cholestene-3-hemisuccinate (CHEMS) and cholesterol (CHOL) were purchased from Sigma-Aldrich (USA). The lipids 2-dioleoyl-*sn*-glycero-3-phosphoethanolamine (DOPE), 1,2-distearoyl-*sn*-glycero-3-phosphocholine (DSPC), 1,2-distearoyl-*sn*-glycero-3-phosphoethanolamine-N-[methoxy(polyethyleneglycol)-2000] (DSPE-PEG2k) were acquired from Lipoid (Germany). N-hexanoyl-D-erythro-sphingosine (C6-ceramide) and N-stearoyl-D-erythro-sphingosine (C18-ceramide) were acquired from Avanti Polar Lipids (USA). All other chemicals were of analytical grade purity.

### 2.2. Cell culture

The triple-negative breast cancer cell lines MDA-MB-231 (ATCC® HTB-26™), MDA-MB-468 (ATCC® HTB-132™) and Hs578T (ATCC® HTB-126™) were cultured in RPMI 1640 (Sigma-Aldrich, USA), supplemented with 10% (v/v) of heat-inactivated Fetal Bovine Serum (FBS) (Invitrogen, USA), 100 U/mL penicillin, 100  $\mu$ g/mL streptomycin (Sigma-Aldrich, USA). All cell lines were maintained at 37°C in a 5% CO<sub>2</sub> atmosphere up to 1 month (from the original batch) to prevent unwanted mutations. Cells were routinely tested for mycoplasma contamination, following the Center for Neuroscience and Cell Biology (CNC) internal rules, and morphology was assessed by microscopy. Cell lines authentication was performed by Short Tandem Repeat (STR) profiling.

### 2.3. Preparation of liposomes

F3 peptide-targeted liposomes, with or without ceramide, were composed of DOPE:CHEMS:DSPC:CHOL:DSPE-PEG2k:DSPE-PEG2k-F3: C6- or C18-ceramide at 2.66:1.34:2:2:0.62:0.18:2 (18 mol% of C6- or C18-ceramide) or 4:2:2:2:0.62:0.18:0 molar ratio, respectively, and were prepared by the ethanol injection procedure (1 mL/batch) as previously described [20,45,52]. Briefly, ethanolic lipid mixtures were added to 300 mM ammonium sulfate solution (pH 6.0) at 60°C and the resulting liposomes were extruded through two stacked polycarbonate membranes (100 nm pore size) using a LiposoFast Basic mini extruder (Avestin, Canada). The buffer was exchanged in a Sephadex G-50 gel column (Sigma-Aldrich, USA) equilibrated with 25 mM HEPES and 10% (w/v) sucrose buffer (pH 6.5). Encapsulation of DXR was carried out through the ammonium sulfate gradient method, upon incubation with liposomes for 1 h at 60°C. Non-encapsulated DXR was removed using a Sephadex G-50 gel column equilibrated with 25 mM HEPES, 140 mM NaCl buffer (pH 7.4).

## 2.4. Characterization of liposomes

The mean size and polydispersity index (PDI) of F3 peptide-targeted liposomes containing a combination of DXR and C6- or C18-ceramide, at a molar ratio of 1:1 ([F3]L-DC<sub>6</sub>11 and [F3]L-DC<sub>18</sub>11, respectively), was determined by dynamic light scattering, Malvern Zetasizer Nano-S, (Malvern Instruments, Malvern, UK) using a standard laser wavelength of 663 nm. The surface charge (zeta potential) was determined by laser Doppler spectroscopy, ZetaSizer Nano-Z, (Malvern Instruments, Malvern, UK). F3 peptide-targeted liposomes containing DXR alone ([F3]L-D) or C6- or C18-ceramide alone ([F3]L-C<sub>6</sub> or [F3]L-C<sub>18</sub>, respectively) and the non-targeted liposomes containing the referred drug combination (L-DC<sub>6</sub>11 and L-DC<sub>18</sub>11) or only DXR (L-D) were used as controls. Encapsulated doxorubicin was assayed at 492 nm from a standard curve, after liposomal solubilization with 90% absolute ethanol, and the encapsulation efficiency (%) was calculated from the equation  $[(DXR/TL)_{final}/(DXR/TL)_{initial}] \times 100$ , where final and initial stand for the doxorubicin and total lipid quantified following and before liposomal preparation, respectively. Additionally, the stability of [F3]L-D, L-DC<sub>6</sub>11, [F3]L-DC<sub>6</sub>11 and [F3]L-DC<sub>18</sub>11 was evaluated by measuring the mean particle size, PDI, and zeta potential, for samples stored at  $5 \pm 3^\circ\text{C}$  (up to 28 days).

For negative-staining transmission electron microscopy (TEM), 10  $\mu\text{L}$  of liposomal suspensions in 25 mM HEPES, 10% (w/v) sucrose buffer, pH 7.4 were deposited on Formvar/carbon film-coated mesh nickel grids (Electron Microscopy Sciences, Hatfield, PA, USA). The liquid excess was removed with filter paper and 10  $\mu\text{L}$  of 1% (w/v) uranyl acetate was added onto the grids. Image acquisition was carried out on a JEOL JEM 1400 TEM at 120 kV (Tokyo, Japan). Images were digitally recorded using a CCD digital camera (Orius 1100 W, Tokyo, Japan). Liposome diameter was drawn from image analysis using ImageJ software v1.49q (NIH, USA). As additional control, a commercially available non-targeted pegylated liposomal formulation of DXR (Caelyx®) was used as control for TEM analysis.

DXR retention was evaluated following the incubation of an aliquot of [F3]L-D, L-DC<sub>6</sub>11, L-DC<sub>18</sub>11, [F3]L-DC<sub>6</sub>11 or [F3]L-DC<sub>18</sub>11 liposomal formulations in HEPES buffer saline pH 7.4, 90% RPMI 1640 culture medium supplemented with 10% FBS or 90% of non-inactivated bovine serum, at  $37^\circ\text{C}$  and at different timepoints (0, 1, 4, 8 and 24 h). Similar experiments were performed at  $4^\circ\text{C}$  over 28 days. DXR fluorescence dequenching was measured in a Spectramax fluorimeter (MolecularDevices, USA) ( $\lambda_{\text{ex}} = 485 \text{ nm}$ ;  $\lambda_{\text{em}} = 590 \text{ nm}$ ) and DXR retention (% of control) was calculated using the following formula:  $100 - [(TestRFU_n - MeanRFU_0)/(MeanRFU_{ctr} - MeanRFU_0)] \times 100$ , where TestRFU<sub>n</sub> and MeanRFU<sub>0</sub> stand for the fluorescence of tested sample at different time points and time 0 h, respectively, and MeanRFU<sub>ctr</sub> is the fluorescence corresponding to 100% of release, following incubation with 0.25% (v/v) of Triton X-100.

## 2.5. Overall cytotoxic effect of lipid-based formulations and a combination of non-encapsulated doxorubicin and cisplatin

Eight, twelve or sixteen thousand MDA-MB-231, MDA-MB-468 or Hs578T cancer cells/well, respectively, adherent to 96-well plates, were incubated with serial dilutions of F3 peptide-targeted pegylated and pH-sensitive liposomes containing DXR and C6- or C18-ceramide, at a 1:1 molar ratio, [F3]L-DC<sub>6</sub>11 or [F3]L-DC<sub>18</sub>11, respectively, the counterparts encapsulating DXR alone, [F3]L-D, and C6- or C18-ceramide alone, [F3]L-C<sub>6</sub> or [F3]L-C<sub>18</sub>, respectively, and combinations of (non-liposomal) DXR and cisplatin or free DXR or cisplatin, for 4 or 24 h, at  $37^\circ\text{C}$  in an atmosphere of 5% CO<sub>2</sub>. Afterwards, cell culture medium was exchanged for fresh one and the experiment extended up to 96 h. Cell viability was assessed by the resazurin reduction assay, upon monitoring absorbance at 570 nm and 600 nm (background) in a Spectramax Gemini EM (Molecular Devices, USA). Cytotoxicity was calculated from the formula  $[100 - ((Test_{570-600} - CtrNeg_{570-600})/(Ctr_{570-600} - CtrNeg_{570-600})) \times 100]$ , where Test<sub>570-600</sub>, Ctr<sub>570-600</sub> and CtrNeg<sub>570-600</sub> were the

corrected absorbance for treated cells, untreated controls and negative control, respectively [53].

The nature of the interaction between DXR and C6- or C18-ceramide encapsulated in the aforementioned pegylated and pH-sensitive liposomes, functionalized with the nucleolin-binding F3 peptide was based on the determination of the combination index (CI) for each of the aforementioned TNBC cell lines, at the IC<sub>50</sub> (fa<sub>0.5</sub>) or IC<sub>90</sub> (fa<sub>0.9</sub>) of targeted liposomal DXR or targeted liposomal C6- or C18-ceramide. The CI was determined using the median-effect model developed by Chou and Talalay [54–56], as detailed previously by our group [52]. Additionally, the determination of the nature of the interaction between the association of non-encapsulated DXR and cisplatin, two drugs used in clinical practice for the treatment of TNBC [2,57,58], was performed as a control using a similar methodology. A combination index lower, equal or higher than 1 corresponded to a synergistic, additive or antagonistic drug interaction, respectively [54–56].

## 2.6. Evaluation of putative breast cancer stem cell population (ALDH<sup>+/high</sup>)

The impact on the putative breast CSC population (ALDH<sup>+/high</sup>), as determined by the Aldefluor assay) was evaluated by flow cytometry. Briefly, 500 000 of MDA-MB-468 TNBC cells/well, adherent to 6-well plates, were incubated with F3 peptide-targeted liposomes containing DXR and C6- or C18-ceramide (1:1 molar ratio) at 2, 5 or 10  $\mu\text{M}$  of DXR or the (non-liposomal) combination of DXR and cisplatin at 1 and 5 or 2 and 10  $\mu\text{M}$  of DXR and cisplatin, respectively, for 24 h at  $37^\circ\text{C}$  in an atmosphere of 5% CO<sub>2</sub>. Five hundred thousand of MDA-MB-231 or Hs578T TNBC cells, adherent to 6-well plates, were incubated with F3 peptide-targeted liposomal combinations at 2, 5, 10 or 20  $\mu\text{M}$  of DXR. Additionally, MDA-MB-231 cells were incubated with the (non-liposomal) combination at 0.2 and 20 or 1 and 45  $\mu\text{M}$  of DXR and cisplatin, respectively, while Hs578T cells were incubated with 0.2 and 8 or 1 and 20  $\mu\text{M}$  of DXR and cisplatin, respectively, for 24 h at  $37^\circ\text{C}$  in an atmosphere of 5% CO<sub>2</sub>. Afterwards, cell culture medium was exchanged for fresh one and the experiment extended up to 96 h. Then, adherent cells were collected along with the suspended (dead) cells to further evaluate cell death and aldehyde dehydrogenase (ALDH) activity.

Live cells were gated (R2 region, Fig. 5A) with the LIVE/DEAD® protocol (Invitrogen by Thermo Fisher Scientific, USA), out of which ALDH<sup>+/high</sup> putative breast CSCs were identified (R4 or R5 regions, Fig. 5A) with the ALDEFUOR™ protocol, according to the manufacturer instructions (Aldagen by STEMCELL Technologies, Canada). The cell-associated signal was immediately analyzed by flow cytometry in a BD FACSCalibur system (BD Biosciences, USA) and a total of 20000 events were collected. Appropriate controls were used to assure correct compensation of fluorescence signals in each channel. For each tested sample, percentage of ALDH<sup>+/high</sup> cells (R5 region) was calculated from the overall cell population gated in the R2 region. These results were further normalized to the percentage of ALDH<sup>+/high</sup> untreated cells (R4 region), as in Fig. 5B.

## 2.7. Evaluation of mRNA levels of NANOG and OCT4

NANOG and OCT4 mRNA levels were determined on TNBC cell lines MDA-MB-231, MDA-MB-468 and Hs578T, plated as described in the previous section, upon incubation with F3 peptide-targeted liposomes encapsulating DXR and C6- or C18-ceramide, at a 1:1 molar ratio, or a (non-liposomal) combination of DXR and cisplatin, at the concentrations and incubation time also described in the previous section.

Upon cell collection, total RNA isolation was performed using the NucleoSpin® RNA II kit (Macherey-Nagel, Germany). Afterwards, RNA concentration and quality were determined using a NanoDrop 2000 (Thermo Fisher Scientific, USA). Samples presenting a 260/280 ratio under 1.9 were discarded. Samples of total RNA were stored at  $-80^\circ\text{C}$

until use. cDNA was obtained using the NZY First-Strand cDNA Synthesis kit (NZYtech, Portugal) according to the manufacturer instructions, using a UnoCycler Thermal Cycler (VWR, USA). Using species-specific pairs of primers, NANOG and OCT4 gene expression was quantified by qRT-PCR using  $\beta$ -ACTIN or RPS18 as housekeeping genes for data normalization. The primers were obtained from a primer bank data base (<http://pga.mgh.harvard.edu/primerbank/>) and acquired from Integrated DNA Technologies (IDT) (supplementary data Table S1). NZYSpeedy qPCR Green Master Mix (NZYtech, Portugal) was used to perform analysis of samples that were run in StepOnePlus Real Time PCR Detection System (Applied Biosystems, Thermo Fisher Scientific, USA). Data were analyzed using the StepOne software v2.3 and the mRNA fold change was calculated using the  $2^{-\Delta\Delta C_t}$  method.

## 2.8. Evaluation of capability of triple-negative breast cancer cells to form mammospheres

The impact over the mammosphere forming efficiency [MFE (%)] was evaluated after incubation of MDA-MB-468, MDA-MB-231 and Hs578T TNBC cells with F3 peptide-targeted DXR and C6- or C18-ceramide liposomes at 5  $\mu$ M (MDA-MB-468) and 10  $\mu$ M (MDA-MB-231 and Hs578T) of DXR, for 24 h at 37°C. Afterwards, cell culture medium was exchanged for fresh one and the experiment extended up to 96 h.

Detached and washed cells were seeded for mammosphere formation, as previously described [20]. Briefly, 5000 single MDA-MB-231 cells or 10000 MDA-MB-468 and Hs578T cells were seeded in 2 mL Mammocult® Medium supplemented with 4 mg/mL of heparin and 0.5 mg/mL of hydrocortisone (STEMCELL Technologies, Canada) per well, in low-adhesion 6-well plates (Greiner, Austria). For 1<sup>st</sup> generation sphere formation, cells were maintained for 10 days at 37°C and 5% of CO<sub>2</sub>. After that period, mammosphere formation efficiency was assessed upon image acquisition (9 random images per well) using Celena S Digital Imaging System (Logos Biosystems, South Korea) and a TC PlanAchrom 4X/0.13 Ph objective. Image analysis and mammosphere counting was performed using ImageJ software v1.49q (NIH, USA). Mammosphere forming efficiency (%) was calculated from the formula [(number of spheres/number of total events) x100], where total events are a sum of the number of mammospheres and single cells.

## 2.9. Assessment of cellular migration of triple-negative breast cancer cells

MDA-MB-468, MDA-MB-231 and Hs578T TNBC cells were plated at low density (12000; 6000 and 3000 cells/well, respectively) in a  $\mu$ -Slide 8 well ibiTreat (IBIDI, Germany) for single-cell tracking. Following incubation with liposomal formulations as mentioned in the previous section, cell culture medium was exchanged to a serum-free medium (to decrease extent of proliferation) aiming at analyzing individual cellular migration. Time lapse imaging was performed on a Axio Observer Z2 microscope (Carl Zeiss, Germany), coupled to a Axiocam HRm and using an EC-Plan-Neofluar 10x/0.3 objective. Throughout the experiment, cells were kept at 37°C and supplied with 5% CO<sub>2</sub>. Three independent fields of view for each well were chosen and imaged every 10 min, for 15 h (total of 91 slices). Data were analyzed using Manual Tracking plugin (ImageJ software v1.49q), and the resulting data exported to Chemotaxis and Migration Tool 2.0 program, with which trajectories were plotted and velocity ( $\mu$ m/min), accumulated distance ( $\mu$ m) and Euclidean distance ( $\mu$ m) parameters were quantified.

## 3. Results

### 3.1. Physical characterization of pH-sensitive and nucleolin-targeted pegylated liposomal combinations of doxorubicin and C6- or C18-ceramides

Pegylated pH-sensitive liposomal formulations functionalized with the nucleolin-binding F3 peptide, containing a combination of DXR and

a short-chain (C6) or a long-chain (C18) ceramide in a 1:1 molar ratio ([F3]L-DC<sub>6</sub>11 and [F3]L-DC<sub>18</sub>11, respectively) were characterized in terms of mean size, polydispersity index (PDI) and surface charge (zeta potential). F3 peptide-targeted liposomes containing DXR ([F3]L-D) or C6- or C18-ceramide alone ([F3]L-C<sub>6</sub> or [F3]L-C<sub>18</sub>, respectively) and non-targeted liposomes containing DXR alone (L-D) or the combination of DXR and C6- or C18-ceramide, at 1:1 molar ratio (L-DC<sub>6</sub>11 or L-DC<sub>18</sub>11, respectively), were used as controls. Furthermore, characterization of morphology by transmission electron microscopy (TEM) was performed and, as additional control, a commercially available pegylated non-targeted liposomal formulation containing DXR alone (Caelyx®) was used.

Measurements by dynamic light scattering following preparation demonstrated that [F3]L-DC<sub>6</sub>11 and [F3]L-DC<sub>18</sub>11 presented a medium size of 113.8 and 114.5 nm, respectively, and a PDI of 0.104 and 0.140, respectively (Fig. 1A). These results were consistent with the measurements of transmission electron microscopy (TEM) for [F3]L-DC<sub>6</sub>11 ( $\mu_z = 110.5$ ; 95.4<sup>25th</sup> – 125.5<sup>75th</sup>) (Fig. 1B) indicating that samples have a monodisperse particle size distribution. These characteristics were also comparable with the mean size and PDI presented by the targeted counterparts containing DXR alone, [F3]L-D, (121.8 nm and 0.103, respectively), C6-ceramide alone, [F3]L-C<sub>6</sub>, (123.8 nm and 0.225, respectively) or C18-ceramide alone, [F3]L-C<sub>18</sub>, (81.8 nm and 0.126, respectively) (Fig. 1A). As expected, non-targeted liposomes, without the functionalization of F3 peptide at the PEG extremity, and containing DXR alone (L-D) or the combination of DXR and C6- or C18-ceramide, at a molar ratio of 1:1 (L-DC<sub>6</sub>11 and L-DC<sub>18</sub>11, respectively), presented lower mean size (97.0, 83.7 or 103.2 nm, respectively) and PDI (0.076, 0.065 or 0.085, respectively) than the targeted counterparts (Fig. 1A).

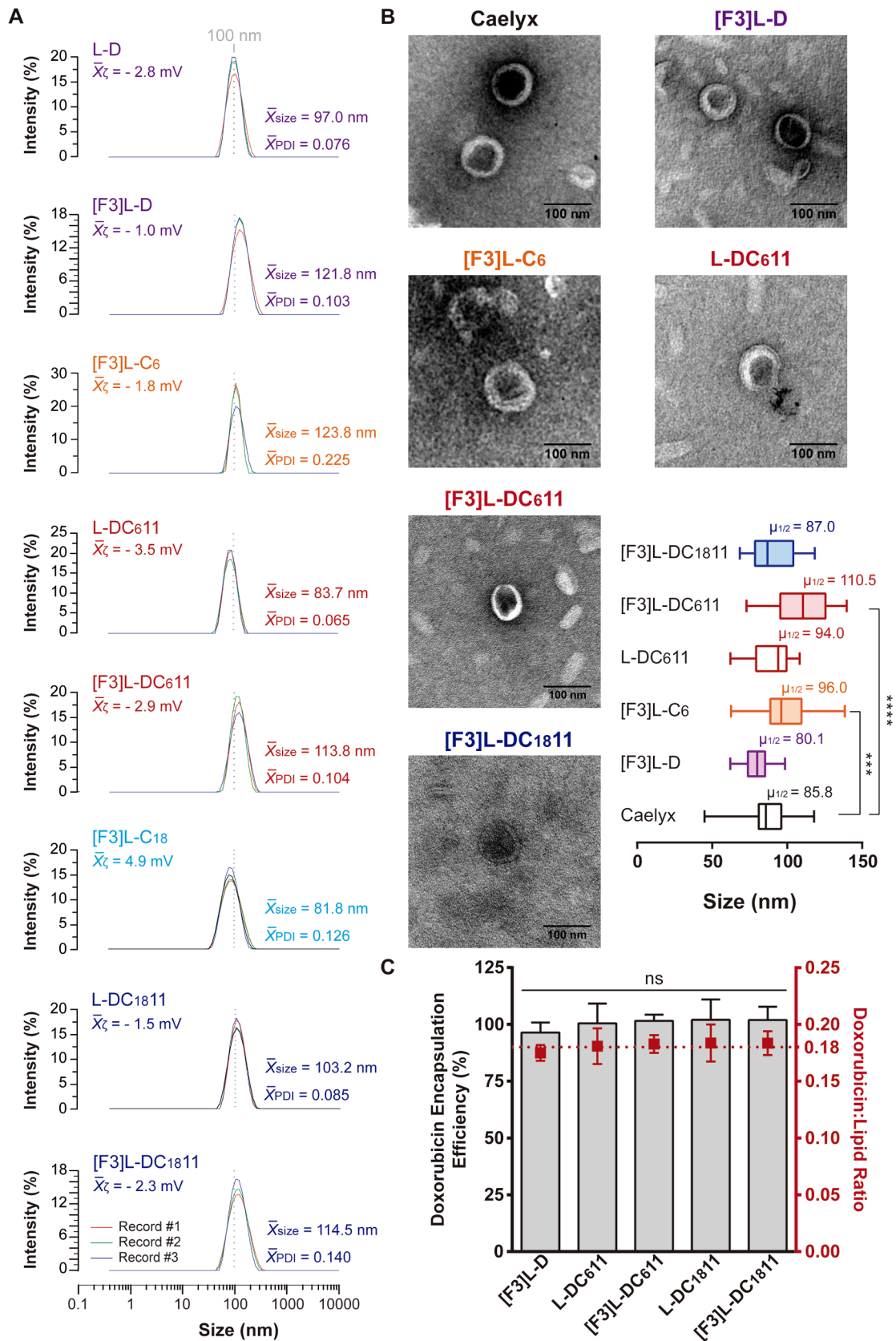
Measurements of zeta potential evidenced that the surface charge of [F3]L-DC<sub>6</sub>11 and [F3]L-DC<sub>18</sub>11 was close to neutrality (–2.9 and –2.3, respectively), as for targeted counterparts containing one drug alone ([F3]L-D: –1.0; [F3]L-C<sub>6</sub>: –1.8; [F3]L-C<sub>18</sub>: 4.9) and non-targeted (L-D: –2.8; L-DC<sub>6</sub>11: –3.5; L-DC<sub>18</sub>11: –1.5) controls (Fig. 1A).

Characterization by TEM demonstrated that [F3]L-DC<sub>6</sub>11 and [F3]L-DC<sub>18</sub>11 presented a spherical shape similar to controls, including Caelyx® (Fig. 1B). All liposomal formulations presented a homogeneous size distribution between 73.8<sup>25th</sup> – 125.5<sup>75th</sup> ( $\mu_z = 80.1$  – 110.5). Additionally, an electron-opaque core was more pronounced in [F3]L-DC<sub>6</sub>11 and [F3]L-DC<sub>18</sub>11 than the counterpart containing only C6-ceramide ([F3]L-C<sub>6</sub>) and similar to control liposomal formulations containing DXR, including Caelyx® (Fig. 1B).

Doxorubicin encapsulation efficiency was close to 100%, at a doxorubicin:lipid ratio (0.18), regardless of the presence of C6- or C18-ceramide in the liposomal bilayer (Fig. 1C).

All liposomal formulations, regardless of the presence of C6- or C18-ceramide, either targeted or non-targeted, presented a similar extent of drug retention (between 95 and 105%), at 37°C for up to 24 h, in different incubation media, including RPMI 1640 cell culture medium supplemented with 10% FBS, reflecting the conditions used in *in vitro* studies (Fig. 2A). Similar observations were extended to the experiments performed at 4°C, over 28 days (Fig. 2B).

F3 peptide-targeted liposomal formulations containing a combination of DXR and C6- or C18-ceramide, at a 1:1 molar ratio, revealed also to be stable in terms of mean size, polydispersity index and zeta potential ( $\zeta$ ), upon storage at 5  $\pm$  3°C for up to 28 days. The only exception refers to the increase in the polydispersity index of [F3]L-DC<sub>18</sub>11 (Fig. 3). A similar trend was observed for F3 peptide-targeted liposomes containing DXR alone ([F3]L-D) or the non-targeted counterpart containing a combination of DXR and C6-ceramide, at a 1:1 molar ratio (L-DC<sub>6</sub>11). The overall analysis of independent batches as reported in Figs. 1 and 3 suggested a surface charge close to neutrality for all liposomal formulations tested. These observations were in accordance with previously characterized GMP-grade batch of F3 peptide-targeted liposomes containing DXR alone (mean size of 91.2 nm, polydispersity index of 0.036  $\pm$  0.006 and zeta potential of +4.9  $\pm$  0.2 mV [59]), which



(caption on next page)

**Fig. 1.** Characterization of nucleolin-targeting liposomal combinations of doxorubicin and/or ceramides with different alkyl chain lengths. A, representative intensity-weighted (%) dynamic light scattering histograms (3 records) of F3 peptide-targeted liposomes containing the combination of DXR and C6- or C18-ceramide, at a molar ratio of 1:1 ([F3]L-DC<sub>6</sub>11 and [F3]L-DC<sub>18</sub>11, respectively). F3 peptide-targeted liposomes containing DXR alone ([F3]L-D) or C6- or C18-ceramide alone ([F3]L-C<sub>6</sub> or [F3]L-C<sub>18</sub>, respectively) and non-targeted liposomes containing DXR alone (L-D) or the combination of DXR and C6- or C18-ceramide, at a molar ratio of 1:1 (L-DC<sub>6</sub>11 or L-DC<sub>18</sub>11, respectively), were used as controls. The mean ( $\bar{x}$ ) size, polydispersity index (PDI) and zeta potential ( $\zeta$ ) values are representative of one batch of liposomes. Dotted lines represent a mean size of 100 nm. B, representative microphotographs of structural morphology, obtained by transmission electron microscopy, and size distribution analysis of [F3]L-DC<sub>6</sub>11 and [F3]L-DC<sub>18</sub>11. [F3]L-D, [F3]L-C<sub>6</sub>, L-DC<sub>6</sub>11 and a commercially available non-targeted pegylated liposomal formulation of DXR (Caelyx®) were used as controls. Data are represented as the minimum to maximum liposomal size distribution, with the box width and the line (inside the box) representing 25th-75th percentile interval and median ( $\mu_{50}$ ), respectively (n = 16–75; one-way ANOVA with Tukey's multiple comparisons post-test; \*\*\*p < 0.001 and \*\*\*\*p < 0.0001). C, Doxorubicin encapsulation efficiency and doxorubicin:lipid ratio of [F3]L-D, L-DC<sub>6</sub>11, L-DC<sub>18</sub>11, [F3]L-DC<sub>6</sub>11 and [F3]L-DC<sub>18</sub>11. Data represent the mean  $\pm$  SEM (n = 2–6; one-way ANOVA with Tukey's multiple comparisons test, ns p > 0.05).

demonstrated tumor targeting properties upon intravenous administration [59]. Overall, [F3]L-DC<sub>6</sub>11 and [F3]L-DC<sub>18</sub>11 presented adequate features for intravenous administration.

### 3.2. Liposomal co-encapsulation of doxorubicin and C6- or C18-ceramides, targeted to nucleolin: Impact on the nature of drug interaction

The nature of the interaction of a combination of DXR and a short-chain or a long-chain ceramide (C6- or C18-ceramide, respectively) in a 1:1 molar ratio, co-encapsulated in pegylated pH-sensitive liposomes, functionalized with the nucleolin-binding F3 peptide was assessed in TNBC cell lines (MDA-MB-468, MDA-MB-231 and Hs578T). As a control, a non-liposomal combination of DXR and cisplatin, two drugs used in clinical practice for the treatment of TNBC, was used [2,57,58]. Herein, a new presentation strategy was adopted (Fig. 4), in order to clearly communicate the determined combination index values and facilitate its analysis. In Fig. 4, the arc segment length encodes the combination index value: the smaller the arc, the smaller the combination index value. Additionally, the arc colors reflected different drug interactions/combination indexes: < 1, synergism (light green) or = 1, additivity (light gray).

In fact, the combinations DXR/C6- or C18-ceramide at the referred molar ratio, at death fractions of either 0.5 (fa 0.5) or 0.9 (fa 0.9), at 4 or 24 h incubation, enabled a synergistic drug interaction in all cell lines tested (Fig. 4).

The association of (non-liposomal) DXR and cisplatin, against Hs578T cells displayed mostly additive interactions, excepting at a death cell fraction of 0.9, at 24 h incubation. Under these conditions, the same nature of interaction was recapitulated in MDA-MB-231 and MDA-MB-468 cells. In these two cell lines, a synergistic interaction was observed any time a death fraction of 0.9 was tested, regardless the incubation time (Fig. 4).

Altogether, these results showed a higher overall cytotoxic potential of the liposomal DXR:C6- or C18-ceramide (1:1 molar ratio) combinations targeted to nucleolin.

In order to clarify the effect of the carrier on cell viability, a systematic analysis was performed as detailed in Table S2. Particularly, the cytotoxicity of non-targeted and F3 peptide-targeted liposomes (without DXR and ceramide, i.e. L and [F3]L), as well as their non-targeted and F3 peptide-targeted liposomal counterparts without DXR (i.e. L-C6 and L-C18, [F3]L-C6 and [F3]L-C18) and with DXR (L-DC<sub>6</sub>11 and L-DC<sub>18</sub>11) was determined. Overall, the vehicle, without C6-ceramide, demonstrated a residual influence on the overall observed viability of the cancer cell lines studied (supplementary data Table S2). This result is somehow in line with the previous demonstration by our group [59] that F3 peptide-targeted liposomes without any drug, and upon intravenous weekly administrations over 4 weeks, had no or residual impact on body weight (in rats and dogs, respectively) and on haematological/chemistry parameters, relative to saline. A similar result was observed upon incorporation of C18-ceramide (supplementary data Table S2). In contrast, C6-ceramide has influenced significantly the overall cytotoxicity (Table S2). In fact, C6-ceramide has been associated with a rapid transbilayer diffusion upon contacting with other phospholipid bilayers [40,60], in contrast with a long-chain sphingolipid, as C18-ceramide

[36], and in line with our demonstration that liposomal C6-ceramide cellular uptake by nucleolin-overexpressing cancer cells was F3 peptide ligand-independent [45].

### 3.3. Differential impact of liposomal combinations of doxorubicin and ceramides of different alkyl lengths (C6 versus C18), targeted to nucleolin, on the percentage of viable ALDH<sup>+/high</sup> putative cancer stem cells

After demonstrating both the synergistic potential and underlying cytotoxicity associated with the intracellular delivery of the combinations comprising DXR and C6- or C18-ceramide, at 1:1 molar ratio, the impact of the different drug combinations against a challenge cell subpopulation as the putative triple negative breast CSC population (defined as ALDH<sup>+/high</sup>) was assessed by flow cytometry [9,10], along with bulk cell death, using a gating strategy (Fig. 5A) as described in Materials and Methods. The effect of each one of the liposomal and non-liposomal drug combinations on the percentage of viable ((R5/R2)  $\times$  100, Fig. 5A) ALDH<sup>+/high</sup> cells (further normalized to the percentage of ALDH<sup>+/high</sup> untreated cells, (R5/R2)/R4 regions, as in Fig. 5B–D, gray axis), were tested at the corresponding previously determined applied treatments at the IC<sub>50</sub> and IC<sub>90</sub> (the lowest and highest values indicated in Fig. 5 caption), along with intermediate values, over 24 h at 37°C. As CSCs have been described to be more resistant to conventional chemotherapy [5,6], drug concentrations highlighted in Fig. 5A were chosen based on their similar extent of activity (IC<sub>90</sub>) against bulk MDA-MB-468 cancer cells, to assess whether there is an enrichment of CSCs, defined as ALDH<sup>+/high</sup>.

MDA-MB-468 cells provided the most striking result among all the cell lines tested. Increasing concentrations of DXR/C18- or C6-ceramide targeted liposomal combinations enabled a maximum of bulk cell death up to 89.1 and 98.8%, along with a 2.9- and 6.2-fold decrease of the percentage of viable ALDH<sup>+/high</sup> putative CSCs (Fig. 5B). In any other of the cell lines tested, have the targeted combinations enabled a decrease of the percentage (fold-change) of viable ALDH<sup>+/high</sup> cells. In MDA-MB-231 the fold change relative to untreated percentage of viable ALDH<sup>+/high</sup> cells remained unchanged for both targeted combinations, although in the one with C6-ceramide (synergistic interaction; Fig. 4), was higher than untreated cells and in contrast with the result provided by the combination with C18-ceramide (Fig. 5C). This has actually likely to do with the higher level of (bulk) cell death (R3 region) provoked by the former combination (up to 87.1%) relative to the latter (up to 53.0%), which enabled a higher extent of selection of viable ALDH<sup>+/high</sup> cells. In Hs578T cells, with maximum levels of (bulk) cell death higher than 90%, an enrichment of viable ALDH<sup>+/high</sup> cells was observed, as the concentration of the targeted combinations increased (Fig. 5D). The ratio (fold-change) lower than 1 suggested a level of ALDH<sup>+/high</sup> cells lower than in untreated cells (Fig. 5D). In respect to the non-liposomal DXR/cisplatin combination, increasing concentrations enabling higher (bulk) cell death were paralleled by a 1.5-, 3.4- and 1.6-fold increase of the percentage of viable ALDH<sup>+/high</sup> cells relative to the untreated control, in MDA-MB-468, MDA-MB-231 and Hs578T TNBC cell lines, respectively (Fig. 5B–D).

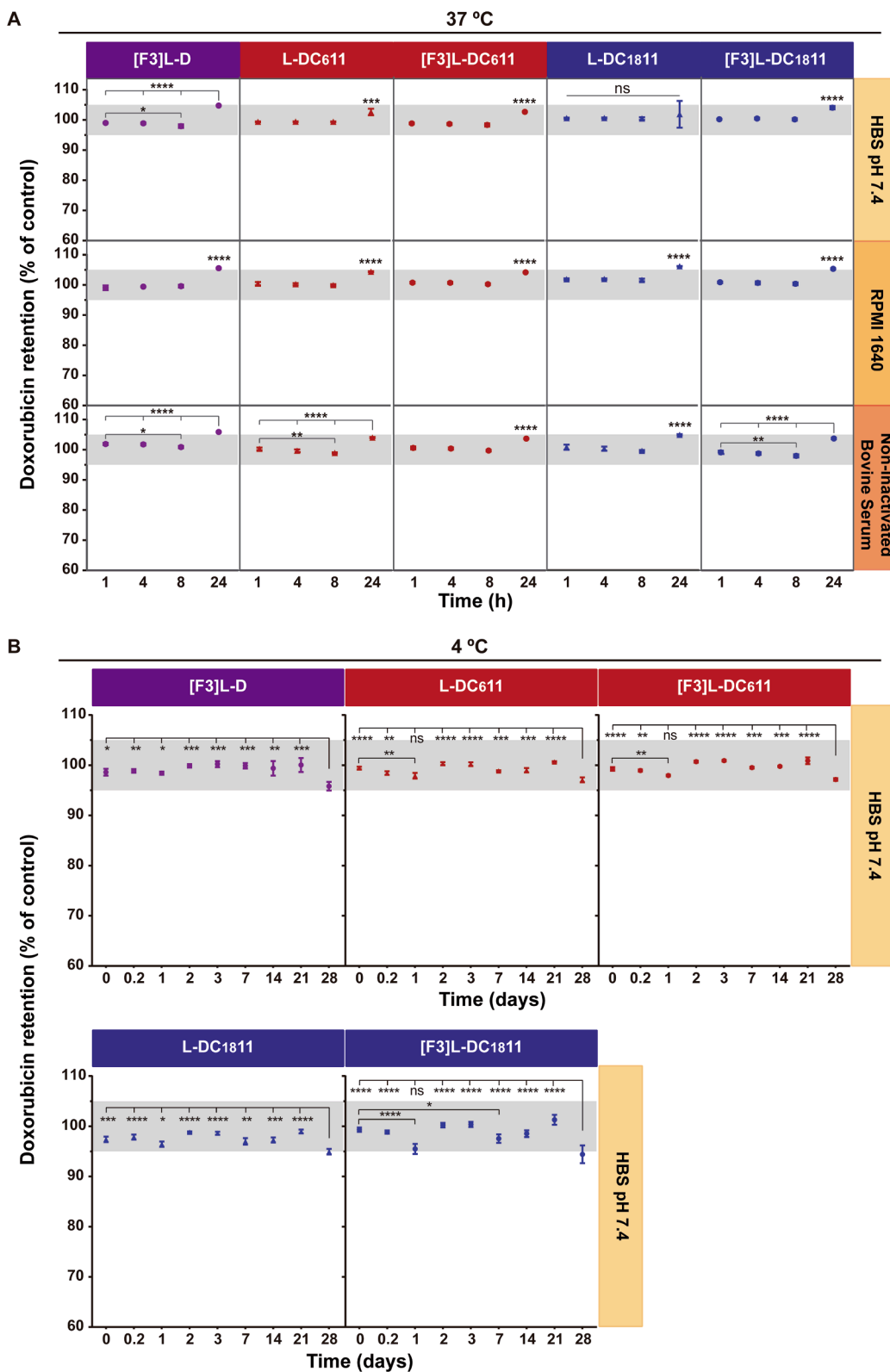


**Fig. 2.** Drug (doxorubicin) retention capacity of different liposomal formulations incorporating doxorubicin alone or in combination with ceramides with different alkyl chain lengths, as a function of time and temperature. Doxorubicin (DXR) retention was evaluated following the incubation of F3 peptide-targeted liposomal formulations containing the combinations of DXR/C6- or C18-ceramide, at a molar ratio of 1:1, [F3]L-DC<sub>611</sub> or [F3]L-DC<sub>1811</sub>, respectively, in the incubation media referred in the figures, at 37°C or 4°C (A and B, respectively). F3 peptide-targeted liposomal formulation containing DXR alone ([F3]L-D) and the non-targeted counterparts containing the combination of DXR/C6- or C18-ceramide, at a 1:1 molar ratio (L-DC<sub>611</sub> or L-DC<sub>1811</sub>, respectively) were used as controls. The gray area delineates a drug retention interval between 95 and 105%. Data represent the mean ± SD (n = 3; one-way ANOVA with Tukey’s multiple comparisons test, ns p > 0.05, \*p < 0.05, \*\*p < 0.01, \*\*\*p < 0.001, \*\*\*\*p < 0.0001).

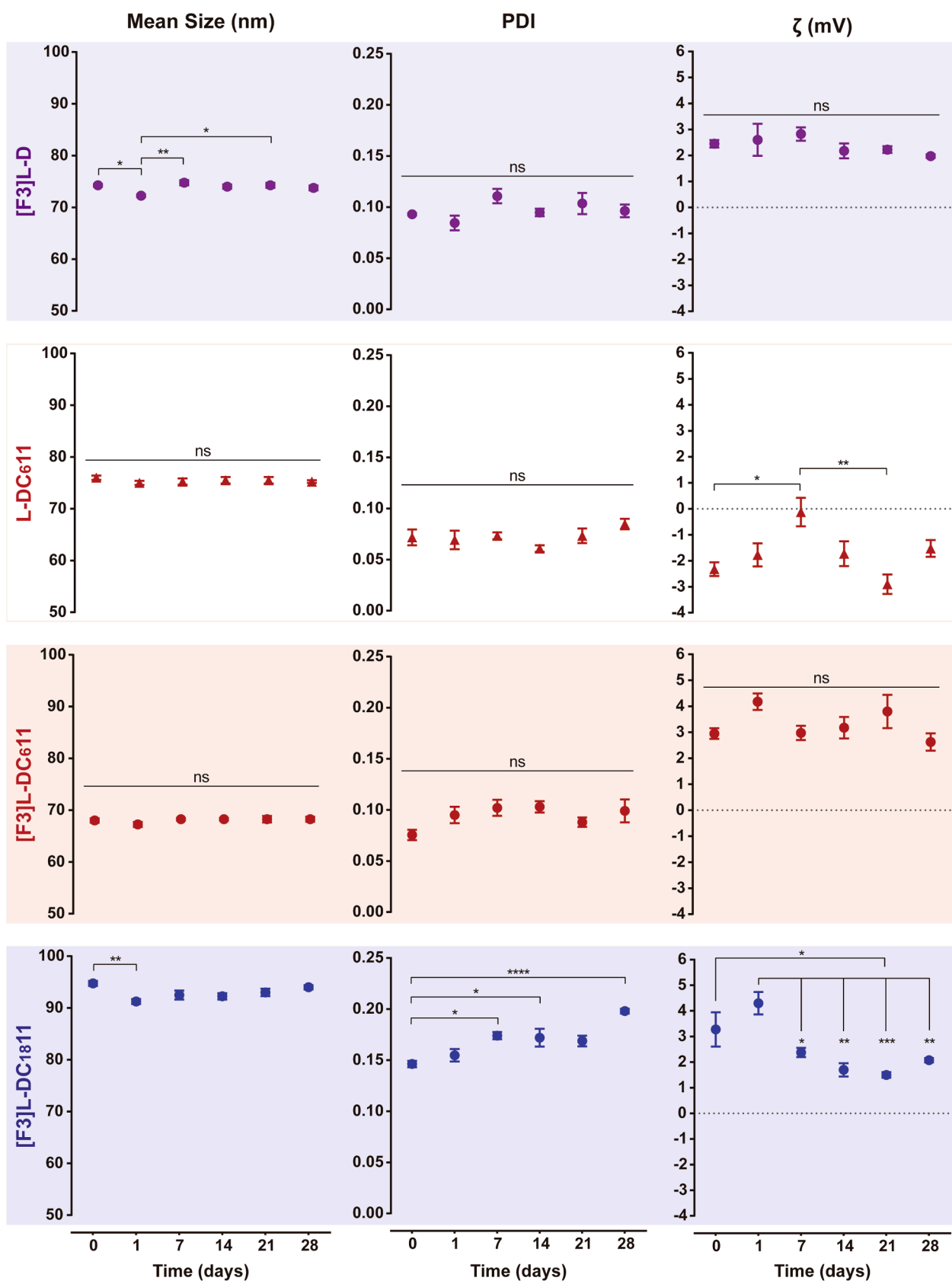


**Fig. 3.** Physical stability of nucleolin-targeting liposomal combinations of doxorubicin and ceramides with different alkyl chain lengths. Time-lapse analysis of mean size, polydispersity index (PDI) and zeta potential ( $\zeta$ ) upon storage of F3 peptide-targeted liposomal formulations containing the combinations of DXR/C6- or C18-ceramide, at a molar ratio of 1:1, [F3]L-DC<sub>6</sub>11 or [F3]L-DC<sub>18</sub>11, respectively, at 5 ± 3°C up to 28 days. F3 peptide-targeted liposomal formulation containing DXR alone ([F3]L-D) and the non-targeted counterpart containing the combination of DXR/C6-ceramide, at a 1:1 molar ratio (L-DC<sub>6</sub>11) were used as controls. Each data point represents the mean value ± SEM (n = 4; one-way ANOVA with Tukey's multiple comparisons test, ns p > 0.05, \*p < 0.05, \*\*p < 0.01, \*\*\*p < 0.0001).

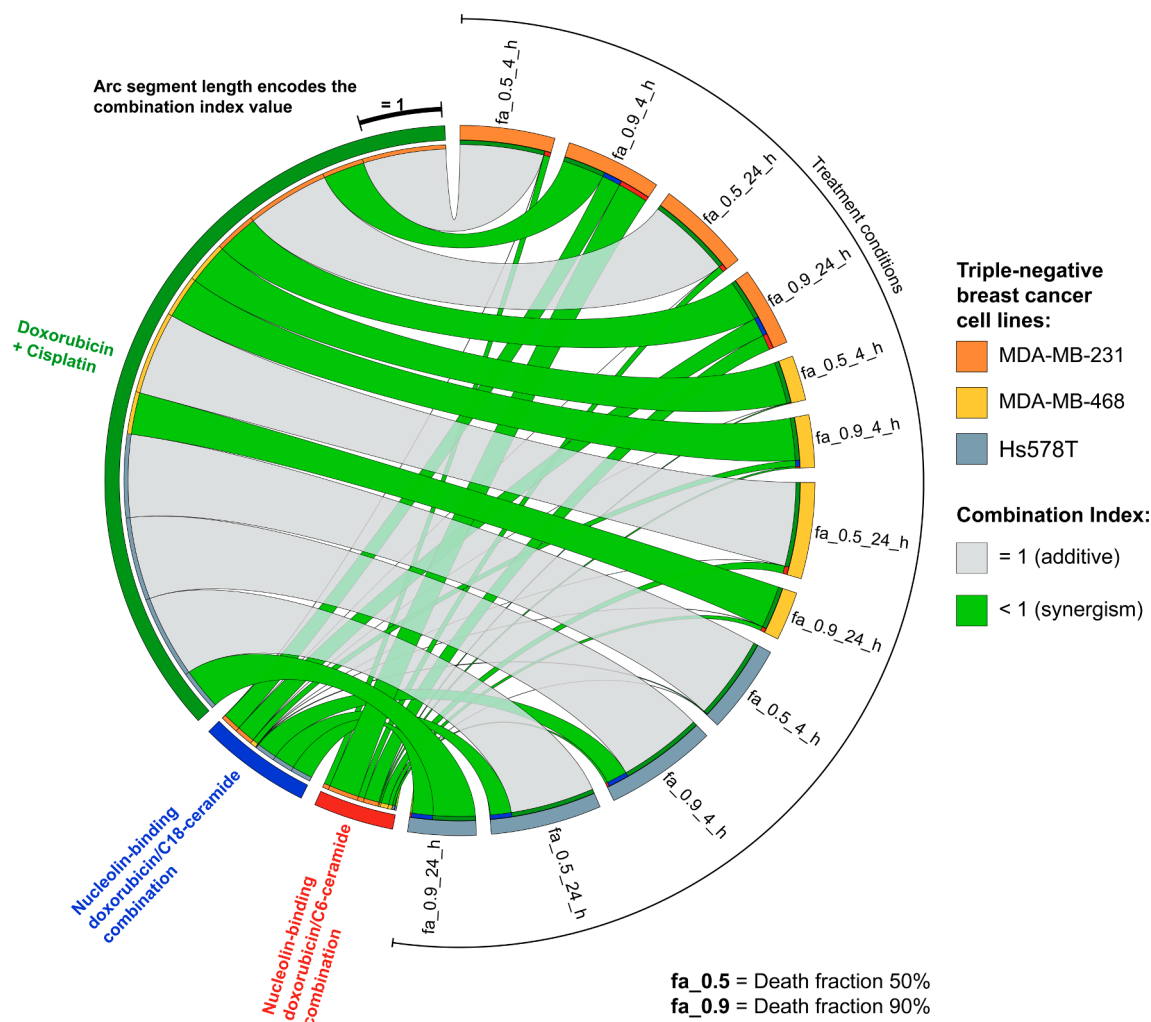


**Fig. 4.** Determination of the nature of interaction between nucleolin-targeting liposomal combinations of doxorubicin and ceramides with different alkyl chain lengths. The nature of the interaction between nucleolin-targeting liposomal DXR co-encapsulated with C6- or C18-ceramide ([(DXR + Cer]<sub>combined</sub>/[(DXR]<sub>alone</sub> + [Cer]<sub>alone</sub>)) against triple-negative breast cancer cell lines MDA-MB-231, MDA-MB-468 and Hs578T, at liposomal DXR and C6- or C18-ceramide IC<sub>50</sub> (fa\_0.5) or IC<sub>90</sub> (fa\_0.9). Additionally, the combination index of DXR combined with cisplatin (Cis) was also determined ((DXR + Cis)<sub>combined</sub>/[(DXR]<sub>alone</sub> + [Cis]<sub>alone</sub>)) against the same cell lines, at free DXR and cisplatin IC<sub>50</sub> (fa\_0.5) or IC<sub>90</sub> (fa\_0.9). The arc segment thickness and color encode for the combination index value (according to scale) and underlying drug interaction: < 1, synergism (light green) or = 1, additivity (light gray).

### 3.4. Effect of liposomal combinations of doxorubicin and ceramides of different alkyl chain lengths (C6 versus C18), targeted to nucleolin, on mRNA levels of pluripotency transcripts factors in (bulk) triple-negative breast cancer cells

The effect of liposomal and non-liposomal combinations on ALDH<sup>+</sup>/<sup>high</sup> putative triple-negative breast CSCs was further extended at the molecular level, upon assessing the mRNA level of pluripotency transcription factors OCT4 and NANOG, at the concentrations and incubation time tested in the previous section.

In MDA-MB-468 cells, the mRNA levels of OCT4 and NANOG, normalized to untreated cells, were lower than 1.4, within the range of tested concentrations of targeted liposomal combination of DXR and C6- or C18-ceramide (Fig. 6A and B). This result was in agreement with the decrease of the percentage of ALDH<sup>+</sup>/<sup>high</sup> MDA-MB-468 cells, relative to the untreated counterpart, previously reported (Fig. 5B). In MDA-MB-231 cells, an average of OCT4 mRNA 2.4–2.9-fold change was evidenced for the lowest concentrations tested and regardless the presence of C6- or C18-ceramide in the F3 peptide-targeted liposomal combination. At the mRNA NANOG level, at the lowest concentrations of the targeted liposomal combination containing C18-ceramide, a maximum 4.8-fold change was reached, decreasing markedly as the incubated

concentration increased (Fig. 6A and B). In Hs578T cells 1.4–2.1-fold (for both targeted liposomal formulations) and 1.9–3.4-fold (for C6-ceramide containing liposomes) changes were observed for OCT4 and NANOG mRNA levels, respectively. Interestingly, as the concentrations of targeted liposomes containing C18-ceramide increased, a trend on the increase of NANOG mRNA was evident (Fig. 6A and B), in line with the possible enrichment of ALDH<sup>+</sup>/<sup>high</sup> Hs578T cells previously reported (Fig. 5D).

In respect to the non-liposomal combination of DXR and cisplatin, a general trend was observed where the increase of drug concentration was accompanied by an augment of OCT4 and NANOG mRNA levels (Fig. 6A and B), in line with the previously observed enrichment of ALDH<sup>+</sup>/<sup>high</sup> cells, in all cell lines tested (Fig. 5B–D).

### 3.5. Impact of the intracellular delivery of the liposomal combinations comprising doxorubicin and C6- or C18-ceramide on the phenotype of triple-negative breast cancer cells

Results from previous sections suggested that regardless of the nature of interaction of a drug combination (synergistic or additive) assessed in bulk cancer cell lines, the impact on ALDH<sup>+</sup>/<sup>high</sup> putative CSCs could diverged, particularly in the case of liposomal combinations, depending

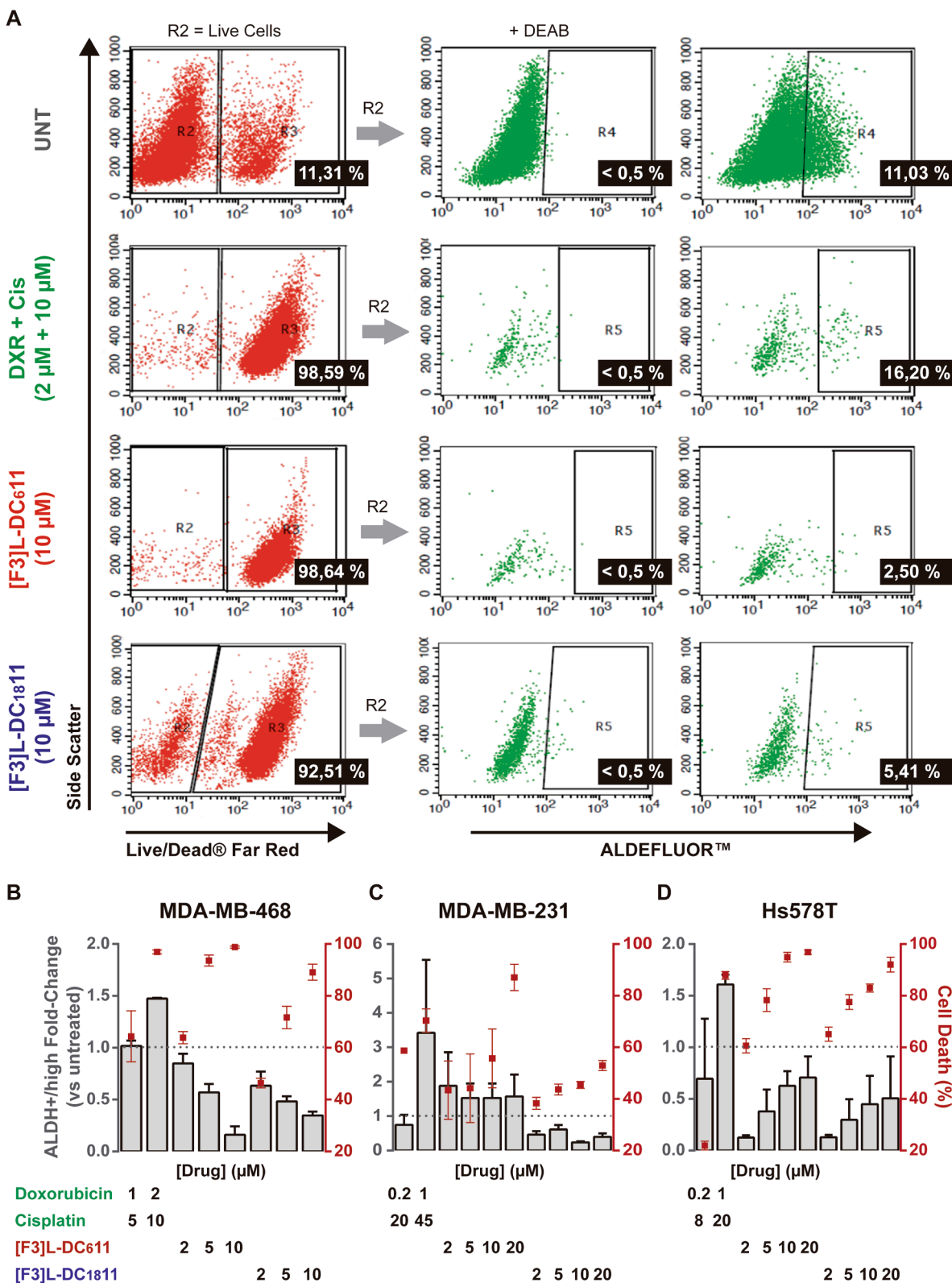


**Fig. 5.** Effect of liposomal and non-liposomal drug combinations on ALDH<sup>+/high</sup> putative cancer stem cell population and extent of death of triple-negative breast cancer bulk cell lines. MDA-MB-468, MDA-MB-231 and Hs578T cells were incubated with the indicated concentrations of free (non-encapsulated) doxorubicin (DXR)/cisplatin (Cis) and F3 peptide-targeted liposomal DXR and C6- or C18-ceramide combinations, for 24 h. The impact on the putative CSC population (ALDH<sup>+/high</sup>, as determined by the Aldefluor® assay) was evaluated by flow cytometry after 96 h, while cell death was determined with the Live/Dead™ assay at the same time-point. A, illustrates the representative region criteria for the identification of viable ALDH<sup>+/high</sup> putative CSC population (DEAB – diethylaminobenzaldehyde, a specific inhibitor of ALDH activity) in MDA-MB-468 cells. B, C and D, represent the relation between cell death (%) (red squares) and the fold-change of ALDH<sup>+/high</sup> population (gray bars) for MDA-MB-468, MDA-MB-231 and Hs578T cells, respectively, relative to untreated (UNT) cells. Dotted lines represent an ALDH<sup>+/high</sup> fold-change (vs untreated) equal to 1. [F3]L-DC<sub>611</sub> and [F3]L-DC<sub>1811</sub> represent the liposomal targeted combination of DXR and C6- or C18-ceramide (at 1:1 molar ratio), respectively.

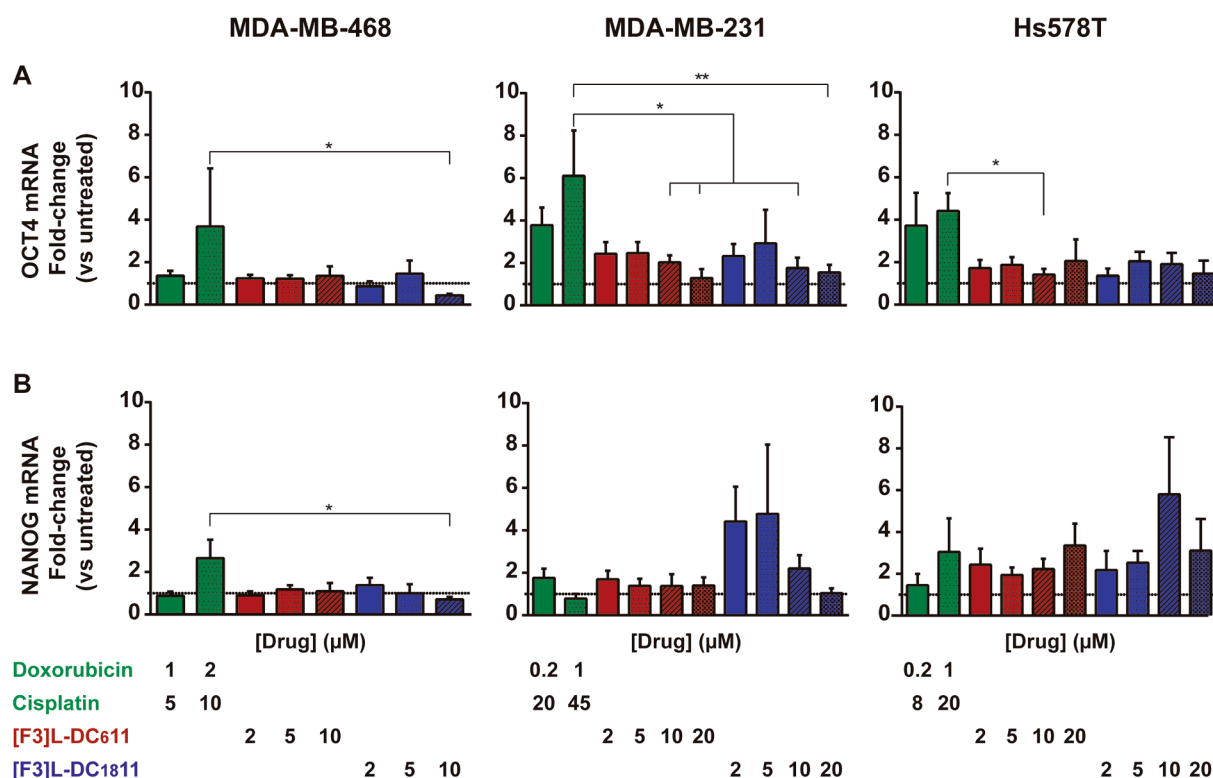


**Fig. 6.** Effect of different non-liposomal and liposomal drug combinations on OCT4 and NANOG mRNA levels in triple-negative breast cancer cell lines. MDA-MB-468, MDA-MB-231 and Hs578T triple-negative breast cancer cells were incubated with the indicated concentration of free (non-encapsulated) DXR and cisplatin combination or targeted liposomes co-encapsulating DXR and C6-ceramide ([F3]L-DC<sub>611</sub>), or C18-ceramide ([F3]L-DC<sub>1811</sub>), at 1:1 molar ratio, for 24 h. A and B, represent the relative mRNA fold-change (vs untreated) of OCT4 and NANOG, respectively. Dotted lines represent a mRNA fold-change (vs untreated) equal to 1. Data represent mean ± SEM (n = 4, Mann-Whitney test; \*p < 0.05, \*\*p < 0.01).

on the cell line tested (Fig. 5). In this respect, for example, an increased concentration (from 50 to 90% cell death) of the targeted liposomal synergistic combination of DXR and C6-ceramide, at 1:1 molar ratio, regardless the cell death fraction and cell line tested (Fig. 4), enabled a decrease or possible enrichment of ALDH<sup>+/high</sup> putative cancer stem MDA-MB-468 (Fig. 5B) or Hs578T (Fig. 5D) cells, respectively. At this stage, it was therefore important to evaluate the impact of the intracellular delivery of the liposomal combinations comprising DXR and C6- or C18-ceramide on the phenotype of TNBC cells as, for example, on the mammosphere forming efficiency and cellular migration.

The result on the putative enrichment of ALDH<sup>+/high</sup> putative cancer stem Hs578T (Fig. 5D) cells, led us to test a drug concentration (as a function of DXR) enabling a fraction of cell death of 70% (that depended on the cell line sensitivity to DXR). This level of cell death provided an appropriate cell density in the end of the experiment to make the necessary assessments. In both set of experiments, incubations were performed for 24 h.

The mammosphere forming efficiency (MFE) was used as a measure of stemness presented by TNBC cell lines. Regarding first generation mammospheres, as described in *Materials and Methods*, a decrease of MFE of MDA-MB-468 cells was observed, upon incubation with the liposomal combinations of DXR and C6- or C18-ceramide (MFE of 6.1 and 5.1%, respectively) relative to the untreated control (MFE of 15.7%, p < 0.01 or 0.05, respectively) (Fig. 7). A similar pattern of significant MFE impairment enabled by the targeted liposomal formulations, relative to untreated cells, was observed with the MDA-MB-231 and Hs578T cells, without major differences in the relative extent among C6- and C18-ceramide formulations (Fig. 7), except for Hs578T cells. In these cells, an increase of MFE was observed, upon incubation with the liposomal combination of DXR and C18-ceramide (MFE of 4.0%) relative to the incubation with the liposomal combination of DXR and C6-ceramide (MFE of 1.1%, p < 0.05) (Fig. 7). This result was in line with the

observed trend on the increase of NANOG mRNA (Fig. 6B) and the possible enrichment of ALDH<sup>+/high</sup> Hs578T cells previously reported (Fig. 5D).

The impact of targeted liposomal drug combinations on cell migration was assessed under three components: velocity, accumulated distance and Euclidean distance (length of the straight-line distance connecting the starting and ending points of cell migration). The effect was in fact different depending on the intrinsic phenotype of each cell line (Fig. 8A and B).

On MDA-MB-468 cells, characterized by an epithelial phenotype [61], both C6- and C18-ceramide liposomal combinations enabled a significant decrease in velocity and accumulated distance, relative to untreated control, and at a similar extent among them (Fig. 8B). A similar pattern was observed with the Hs578T cells, characterized by a mesenchymal-like phenotype [62]. The only difference relied at the level of the Euclidean distance, where the formulation incorporating C6-ceramide induced higher reduction of the straight segment of migration than the C18 counterpart (Fig. 8B, p < 0.05). In the case of highly motile MDA-MB-231 cells [61,62], different results were observed (Fig. 8B and three single-cell tracking videos, supplementary videos 1, 2 and 3 available online). Not only significant differences relative to untreated cells were identified for all the three migration parameters assessed, but also the F3 peptide-targeted combination of DXR and C6-ceramide induced a statistically significant decrease on each of those parameters, relative to the C18-ceramide counterpart.

#### 4. Discussion

Cancer is a heterogeneous disease and the tumor microenvironment is constituted by different cells types, including cancer cells, CSCs, endothelial cells, immune inflammatory cells and cancer-associated fibroblasts, that contribute to the tumor pathogenesis [63]. Moreover, a

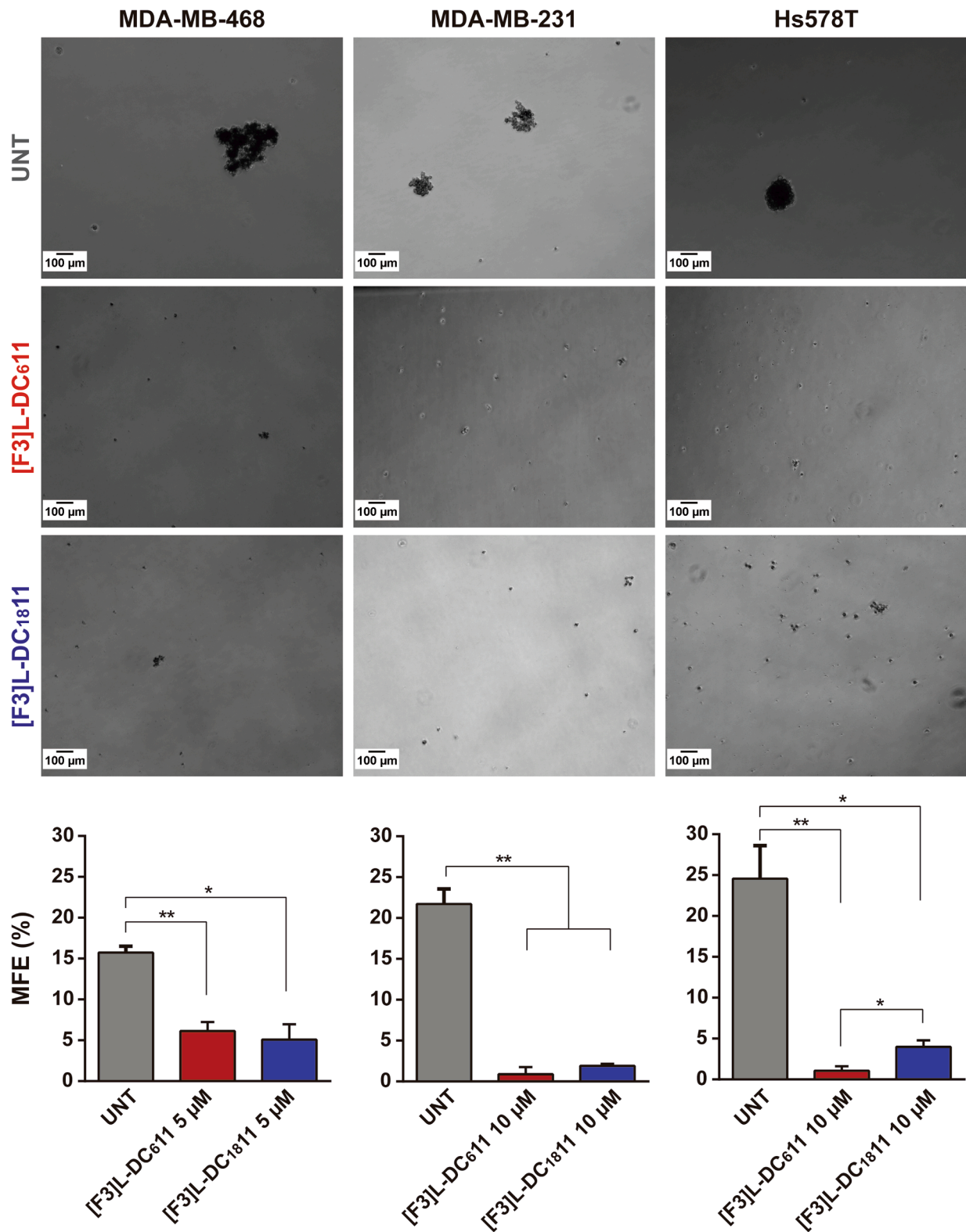


**Fig. 7.** Effect of intracellular delivery of the liposomal combinations comprising doxorubicin and C6- or C18-ceramide on mammosphere forming efficiency [MFE (%)] in triple-negative breast cancer cell lines. MDA-MB-468, MDA-MB-231 and Hs578T cells were incubated with the indicated concentration (corresponding to IC<sub>70</sub>) of targeted liposomal combination of DXR and C6-ceramide ([F3L-DC<sub>611</sub>]), or C18-ceramide ([F3L-DC<sub>1811</sub>]), at 1:1 molar ratio, for 24 h. Afterwards, cell culture medium was exchanged for fresh one and the experiment was extended up to 96 h. After washing, isolated cells were seeded for mammosphere formation. After 10 days, mammospheres >50 μm were counted and the mammosphere forming efficiency [MFE (%)] was calculated (ratio between number of spheres and total number of mammospheres and single cells). Images represent bright-field microscopic images of first generation mammospheres. Data represent mean ± SEM (n = 3, unpaired *t* test with Welch's correction; \**p* < 0.05, \*\**p* < 0.01).

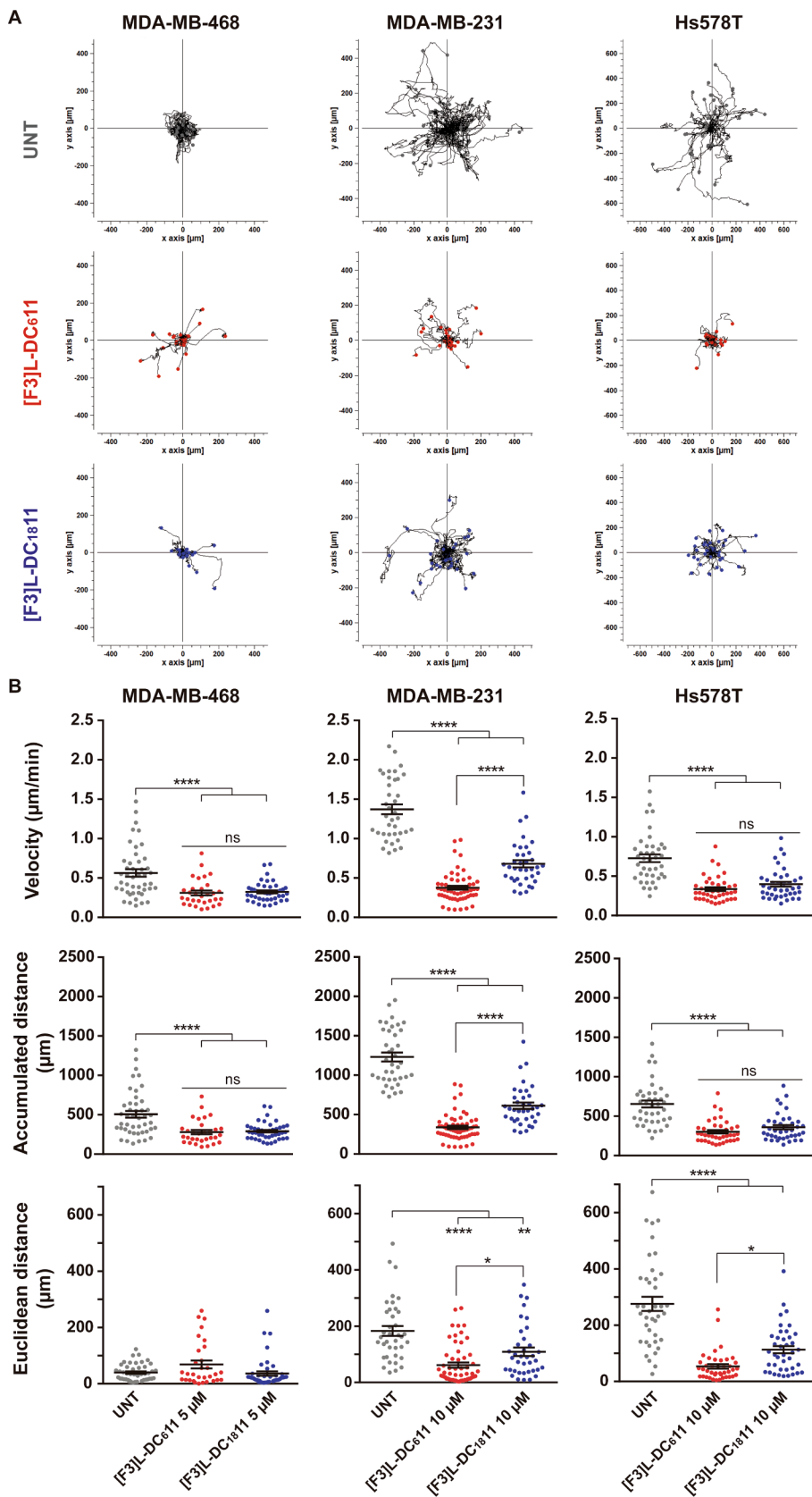


**Fig. 8.** Effect of intracellular delivery of the liposomal combinations comprising doxorubicin and C6- or C18-ceramide on the migration of triple-negative breast cancer cell lines. MDA-MB-468, MDA-MB-231 and Hs578T triple-negative breast cancer cells were incubated with the indicated concentration (corresponding to  $IC_{70}$ ) of targeted liposomal combination of DXR and C6-ceramide ([F3]L-DC<sub>6</sub>11) (red), or C18-ceramide ([F3]L-DC<sub>18</sub>11) (blue), at 1:1 molar ratio, for 24 h. Afterwards, cell culture medium was exchanged for a serum-free medium and time lapse imaging was performed. Three independent fields for each well were chosen and imaged every 10 min, for 15 h. A, represents single cell trajectories, while B, represents scatter dot plots of migratory velocity ( $\mu\text{m}/\text{min}$ ), accumulated distance ( $\mu\text{m}$ ) and Euclidean distance ( $\mu\text{m}$ ) of tracked cells incubated with the F3 peptide-targeted liposomal combinations or untreated (UNT) control (grey). The error bars indicate mean  $\pm$  SEM (total number of cells  $\geq 29$ , from 3 independent experiments; one-way ANOVA with Tukey's multiple comparisons test; ns  $p > 0.05$ , \* $p < 0.05$ , \*\* $p < 0.01$ , \*\*\*\* $p < 0.0001$ ).

complex signaling network of deregulated pathways that control cell growth, viability and motility has been implicated in tumor development and progression [15,63]. It thus recognized that drug combinations targeting different cellular populations and/or signaling pathways are paramount to successfully tackle cancer heterogeneity. In this respect, synergistic interaction of anticancer drugs can provide significant improvements in efficacy and/or dose reduction, while maintaining therapeutic efficacy and avoiding toxicity [54].

Our group had previously shown that intracellular delivery of F3 peptide-targeted liposomal drug combinations into bulk cells could significantly influence the nature of the drug interaction, upon shifting the additive/antagonistic interaction of DXR:C6-ceramide in its free/non-liposomal form [52]. Herein, intracellular delivery of DXR/C6- or C18-ceramide combinations, at a molar ratio of 1:1, mediated by the F3 peptide/nucleolin system enabled a synergistic drug interaction in all conditions and TNBC cell lines tested (Fig. 4). However, the encapsulation of DXR/C6-ceramide combination (1:1 molar ratio) resulted, in general, in lower combination indexes (smaller arcs, Fig. 4). The cytotoxic potency of C6-ceramide higher than C18-ceramide can be explained by the potential role of C6-ceramide in sensitizing cancer cells of diverse histological origin to chemotherapeutic agents, such as DXR, by enhancing DXR-induced activation of adenosine monophosphate activated protein kinase, leading to apoptosis of cancer cells [38].

Notwithstanding the wide synergistic activity of the DXR/C6- or C18-ceramide targeted combinations determined against the aforementioned bulk TNBC cells, assessment at the level of corresponding putative CSC population (defined as ALDH<sup>+/high</sup>) revealed a cell-dependent effect. CSCs are described as the main responsible for sustaining tumor growth, recurrence of tumors, development of metastasis and resistance to conventional chemotherapy [64,65]. MDA-MB-468 cells, characterized by an epithelial phenotype [61], provided the most remarkable result among all the cell lines tested. Increasing concentrations of DXR/C18- or C6-ceramide targeted liposomal combinations enabled significant bulk cell death, along with a decrease of the percentage of viable ALDH<sup>+/high</sup> putative CSCs, respectively (Fig. 5A and B). In the cell lines characterized by a mesenchymal-like phenotype (MDA-MB-231 and Hs578T) [62], the targeted combinations did not enable a decrease of the percentage (fold-change) of viable ALDH<sup>+/high</sup> cells (Fig. 5C and D). In Hs578T cells an enrichment of viable ALDH<sup>+/high</sup> cells was observed for both types of ceramides, as the concentration of the targeted combinations increased (Fig. 5D). Interestingly also to point out was the fact that only in the case of MDA-MB-231 cells, the percentage of ALDH<sup>+/high</sup> cells exceeded the untreated ones. This was an observation that might be related with lower cell surface density of nucleolin, relative to MDA-MB-468 and Hs578T cancer cells (supplementary Fig. S1). Importantly, the incubation with increasing concentrations of the combination of non-liposomal DXR and cisplatin, associated with increased cytotoxicity against bulk cells, was accompanied by an evident selection of CSCs, as demonstrated by the increasing percentage of viable ALDH<sup>+/high</sup> cells, among all cell lines tested (Fig. 5). This observation was in accordance with CSCs described resistance to conventional chemotherapy [66–68]. In fact, the analysis of breast cancer core biopsies obtained from patients after 12 weeks of treatment with neoadjuvant chemotherapy (docetaxel or DXR and cyclophosphamide) demonstrated increased percentage of the putative breast CSC population CD44<sup>+</sup>/CD24<sup>low</sup> and increased mammosphere formation efficiency relative to paired biopsies from patients before the treatment [66].

OCT4 and NANOG co-expression has been associated with poor prognosis of breast cancer patients [17] and with the maintenance of stemness in pancreatic CSCs [16]. In the breast cancer BT-20 cell line, the double knockdown of OCT4 and NANOG expression in putative CSC population, CD44<sup>+</sup>/CD24<sup>low</sup>, resulted in the downregulation of both mesenchymal markers, as N-cadherin and vimentin, and transcription factors known to facilitate epithelial-to-mesenchymal transition, Slug and Snail [17]. Herein, the assessment of the effect of non-liposomal

combinations at the molecular level, demonstrated a general trend of increased mRNA level of pluripotency transcription factors OCT4 and NANOG, except in the case of MDA-MB-231 cells (Fig. 6A and B). The effect of liposomes functionalized with the nucleolin-binding F3 peptide containing DXR and C6- or C18-ceramide was heterogeneous and thus inconclusive.

Altogether, the previous results indicated that the nature of the interaction of different drug combinations and the underlying cell cytotoxicity assessed at the level of bulk cells is not necessarily recapitulated at the level of the putative CSC population. They emphasize for the first time, to the best of the authors knowledge, the importance of redefining the way the nature of drug interactions (within combinations) is studied. Extending the assessment to CSCs, known to be able to survive following a treatment and further capable of repopulating the tumor, due to self-renewal capacity, leading to tumor recurrence, is of pivotal importance [5,64]. This perspective actually relates with the current clinical experience with Vyxeos®, a liposomal synergistic combination of daunorubicin and cytarabine (1:5 molar ratio) whose nature of drug interaction was also determined in bulk cancer cells [69] by the Chou and Talalay method [55]. In fact, despite the improved median overall survival (OS) and overall remission rate of patients with newly diagnosed secondary acute myeloid leukemia (AML) following treatment with Vyxeos®, relative to the standard-of-care cytarabine plus daunorubicin chemotherapy (7 + 3 regimen) (OS = 9.56 versus 5.95 months and remission rate = 47.7% versus 33.3%, respectively) in a phase III clinical trial [70], their prognosis remained poor. This was likely due to the limited effect of the synergistic drug combination against putative CSC population in AML. This thus supported a phase II clinical trial of CPX-351 combined with gemtuzumab ozogamicin, an antibody-drug conjugate targeted to CD33 [71], in treating patients with relapsed or refractory AML or high-risk myelodysplastic syndrome (NCT03672539). CD33 overexpression was demonstrated in CD34<sup>+</sup>/CD38<sup>-</sup> AML leukemic stem cells relative to normal hematopoietic stem cells [72], suggesting that targeting CD33 could potentially eliminate the putative CSC population in AML [71].

Considering the divergent impact of liposomal combinations comprising DXR and C6- or C18-ceramide on ALDH<sup>+/high</sup> putative CSCs, depending on the cell line tested, their effect on the phenotype of triple-negative breast CSCs as, for example, on the mammosphere forming efficiency and cellular migration, became of high relevance. Sphere-forming assays have been used as an *in vitro* measure of stem cell/early progenitor activity (primary generation of spheres) [12] and the formation of mammospheres in three-dimensional culture is a characteristic of breast CSCs [73,74]. The incubation with the F3 peptide-targeted liposomal combinations of DXR and C6- or C18-ceramide resulted in a decrease of primary mammosphere forming efficiency of all TNBC cell lines tested, relative to untreated control, without major differences in the relative extent among C6- and C18-ceramide formulations, except for Hs578T cells (Fig. 7) where the former was more active than the latter. The inhibitory effect of the referred liposomal targeted combinations of DXR and C6- or C18-ceramide on mammosphere development is in line with previously described induction of cell cycle arrest at the G1 and G2 phases by ceramides in cancer cells, including triple-negative, limiting proliferation [42,75,76]. Moreover, C6-ceramide has demonstrated to downregulate PI3K/Akt pathway [45,46], described to be essential for breast CSCs survival and proliferation [47,49].

Additionally, the impact on the migratory potential of TNBC cells, as an indicator of the invasion and metastatic potential [77], was further assessed for both targeted formulations by live single-cell tracking [78,79]. While they have both enabled a significant decrease in migration velocity and accumulated distance parameters, relative to untreated control, among all the cell lines tested, the impact of the C6- or C18-ceramide combinations depended on the intrinsic phenotype of each cell line (Fig. 8). On MDA-MB-468 cells, characterized by an epithelial (and low motility) phenotype [61], there was no difference between C6-

and C18-ceramide liposomal combinations. On Hs578T cells, characterized by a mesenchymal-like phenotype, and associated with a migratory phenotype [62], there was only a difference on Euclidean distance, favoring the targeted liposomal combination of DXR and C6-ceramide. However, in the case of highly motile MDA-MB-231 cells (higher than Hs578T cells, as in Fig. 8B) [61,62], the F3 peptide-targeted liposomal combination of DXR and C6-ceramide induced a statistically significant decrease on all migration parameters evaluated, relative to the C18-ceramide counterpart. Mechanistically, the intracellular delivery of C6-ceramide mediated by the F3 peptide/nucleolin system into MDA-MB-231 TNBC cells was demonstrated to downregulate PI3K/Akt pathway [45] (in contrast with C18-ceramide, supplementary Fig. S2), which has been implicated in survival and proliferation of breast CSCs [47,49] and breast cancer progression and metastasis [80]. Similarly, transferrin-targeted C6-ceramide liposomes decreased cell motility of (invasive) ovarian cancer SKOV-3 cells, upon reducing the formation of lamellipodia by 60% relative to the counterpart without C6-ceramide, an effect mediated by the downregulation of PI3K/Akt pathway [46]. The decrease of migratory potential enabled by the targeted liposomal combinations is of high relevance in the context of TNBC due to an overall 5-year relapse of 40% associated with metastatic spread [81].

## 5. Conclusion

This work further reinforced the use of sphingolipids, like ceramides, as components of ligand-mediated liposomal combinations containing anthracyclines, as DXR, against TNBC cell lines. In fact, both short (C6) and long (C18) alkyl chain ceramides enabled a synergistic drug interaction in all conditions and (bulk) cell lines tested. The differentiation among these two ceramides was evidenced on the migratory potential of TNBC cells, particularly significant against the highly motile MDA-MB-231 cells. At the molecular level, this difference was supported by the downregulation of the PI3K/Akt pathway enabled by C6-ceramide and in contrast with the C18-ceramide counterpart. The decrease of the migratory potential enabled by the targeted liposomal combinations is of high relevance in the context of TNBC due to the underlying metastatic potential.

Interestingly (and surprisingly), the nature of the drug interaction assessed at the level of bulk cancer cells was not coherently recapitulated upon assessment of the corresponding percentage of viable ALDH<sup>+/high</sup> putative triple-negative breast CSCs. While in epithelial cancer cells (MDA-MB-468) a decrease on the percentage of these subpopulation was observed following incubation with F3 peptide-targeted liposomal combinations, an enrichment of ALDH<sup>+/high</sup> MDA-MB-231 was observed.

Altogether, these results demonstrated that the assessment of the nature of interaction on bulk cells likely does not anticipate the impact on master cellular regulators of tumor relapse as CSCs, suggesting that it should be extended further down to this level.

## Declaration of Competing Interest

The authors declare that they have no known competing financial interests or personal relationships that could have appeared to influence the work reported in this paper.

## Acknowledgments

Ana Filipa Cruz is a student of the Pharmaceutical Sciences PhD program from the Faculty of Pharmacy, University of Coimbra, Coimbra, Portugal, with a fellowship from Fundação para a Ciência e a Tecnologia (FCT): SFRH/BD/85554/2012.

This work was also supported by the European Regional Development Fund (ERDF), through the Centro 2020 Regional Operational Program under project CENTRO-01-0247-FEDER-017646 (ODD4-PEGASEMP), and through the COMPETE 2020 - Operational Program

for Competitiveness and Internationalisation and Portuguese national funds via FCT – , I.P., under projects POCI-01-0145-FEDER-016390 (CancelStem), *Euronanomed* (FCT reference ENMed/0005/2015), CENTRO-01-0145-FEDER-000012-HealthyAging2020, PPBI-POCI-01-0145-FEDER-022122, CIBB (FCT references UIDB/04539/2020 and UIDP/04539/2020), iMed (FCT references UIDB/04138/2020 and UIDP/04138/2020).

Authors acknowledge Nuno Vilaça (Pharm D) from the University Hospital Centre of Coimbra, for providing a sample of (non-liposomal) doxorubicin and cisplatin and pegylated liposomal doxorubicin (Caelyx®), and also Rui Lopes (PhD) and Luisa Cortes (PhD), both from the Center for Neuroscience and Cell Biology, University of Coimbra, for providing scientific and technical support to the determination of cell surface nucleolin and cell migration protocol, respectively.

## Appendix A. Supplementary material

Supplementary data to this article can be found online at <https://doi.org/10.1016/j.ejpb.2022.01.006>.

## References

- [1] A.C. Gregorio, M. Lacerda, P. Figueiredo, S. Simoes, S. Dias, J.N. Moreira, Therapeutic implications of the molecular and immune landscape of triple-negative breast cancer, *Pathol. Oncol. Res.* 24 (2018) 701–716.
- [2] J.H. Park, J.H. Ahn, S.B. Kim, How shall we treat early triple-negative breast cancer (TNBC): from the current standard to upcoming immuno-molecular strategies, *ESMO Open* 3 (2018), e000357.
- [3] G.K. Gupta, A.L. Collier, D. Lee, R.A. Hoefer, V. Zheleva, L.L. Siewertsz van Reesema, A.M. Tang-Tan, M.L. Guye, D.Z. Chang, J.S. Winston, B. Samli, R. J. Jansen, E.F. Petricoin, M.P. Goetz, H.D. Bear, A.H. Tang, Perspectives on triple-negative breast cancer: current treatment strategies, unmet needs, and potential targets for future therapies, *Cancers (Basel)* 12 (2020).
- [4] Y. Octavia, C.G. Tocchetti, K.L. Gabrielson, S. Janssens, H.J. Crijns, A.L. Moens, Doxorubicin-induced cardiomyopathy: from molecular mechanisms to therapeutic strategies, *J. Mol. Cell Cardiol.* 52 (2012) 1213–1225.
- [5] E. Batlle, H. Clevers, Cancer stem cells revisited, *Nat. Med.* 23 (2017) 1124–1134.
- [6] K. Moitra, Overcoming multidrug resistance in cancer stem cells, *Biomed. Res. Int.* 2015 (2015), 635745.
- [7] C.L. Chaffer, N.D. Marjanovic, T. Lee, G. Bell, C.G. Kleer, F. Reinhardt, A. C. D'Alessio, R.A. Young, R.A. Weinberg, Poised chromatin at the ZEB1 promoter enables breast cancer cell plasticity and enhances tumorigenicity, *Cell* 154 (2013) 61–74.
- [8] D.R. Pattabiraman, B. Bieri, K.I. Kober, P. Thiru, J.A. Krall, C. Zill, F. Reinhardt, W.L. Tam, R.A. Weinberg, Activation of PKA leads to mesenchymal-to-epithelial transition and loss of tumor-initiating ability, *Science*, 351 (2016) aad3680.
- [9] A.K. Croker, D. Goodale, J. Chu, C. Postenka, B.D. Hedley, D.A. Hess, A.L. Allan, High aldehyde dehydrogenase and expression of cancer stem cell markers selects for breast cancer cells with enhanced malignant and metastatic ability, *J. Cell Mol. Med.* 13 (2009) 2236–2252.
- [10] C. Ginestier, M.H. Hur, E. Charafe-Jauffret, F. Monville, J. Dutcher, M. Brown, J. Jacquemier, P. Viens, C.G. Kleer, S. Liu, A. Schott, D. Hayes, D. Birnbaum, M. S. Wicha, G. Dontu, ALDH1 is a marker of normal and malignant human mammary stem cells and a predictor of poor clinical outcome, *Cell Stem. Cell* 1 (2007) 555–567.
- [11] M.H. Wright, A.M. Calcagno, C.D. Salcido, M.D. Carlson, S.V. Ambudkar, L. Varticovski, Brca1 breast tumors contain distinct CD44+/CD24- and CD133+ cells with cancer stem cell characteristics, *Breast Can. Res.* 10 (2008) R10.
- [12] E. Pastrana, V. Silva-Vargas, F. Doetsch, Eyes wide open: a critical review of sphere-formation as an assay for stem cells, *Cell Stem Cell* 8 (2011) 486–498.
- [13] C. Scheel, R.A. Weinberg, Cancer stem cells and epithelial-mesenchymal transition: concepts and molecular links, *Semin. Can. Biol.* 22 (2012) 396–403.
- [14] J.E. Visvader, G.J. Lindeman, Cancer stem cells: current status and evolving complexities, *Cell Stem Cell* 10 (2012) 717–728.
- [15] N.A. Fonseca, A.F. Cruz, V. Moura, S. Simoes, J.N. Moreira, The cancer stem cell phenotype as a determinant factor of the heterotypic nature of breast tumors, *Crit. Rev. Oncol. Hematol.* 113 (2017) 111–121.
- [16] Y. Lu, H. Zhu, H. Shan, J. Lu, X. Chang, X. Li, J. Lu, X. Fan, S. Zhu, Y. Wang, Q. Guo, L. Wang, Y. Huang, M. Zhu, Z. Wang, Knockdown of Oct4 and Nanog expression inhibits the stemness of pancreatic cancer cells, *Can. Lett.* 340 (2013) 113–123.
- [17] D. Wang, P. Lu, H. Zhang, M. Luo, X. Zhang, X. Wei, J. Gao, Z. Zhao, C. Liu, Oct-4 and Nanog promote the epithelial-mesenchymal transition of breast cancer stem cells and are associated with poor prognosis in breast cancer patients, *Oncotarget* 5 (2014) 10803–10815.
- [18] A.S. Beltran, A.G. Rivenbark, B.T. Richardson, X. Yuan, H. Quian, J.P. Hunt, E. Zimmerman, L.M. Graves, P. Blanche, Generation of tumor-initiating cells by exogenous delivery of OCT4 transcription factor, *Breast Can. Res.* 13 (2011) R94.
- [19] M. Najafi, B. Farhood, K. Mortezaee, Cancer stem cells (CSCs) in cancer progression and therapy, *J. Cell Physiol.* 234 (2019) 8381–8395.

- [20] N.A. Fonseca, A.S. Rodrigues, P. Rodrigues-Santos, V. Alves, A.C. Gregorio, A. Valerio-Fernandes, L.C. Gomes-da-Silva, M.S. Rosa, V. Moura, J. Ramalho-Santos, S. Simoes, J.N. Moreira, Nucleolin overexpression in breast cancer cell sub-populations with different stem-like phenotype enables targeted intracellular delivery of synergistic drug combination, *Biomaterials* 69 (2015) 76–88.
- [21] S. Christian, J. Pilch, M.E. Akerman, K. Porkka, P. Laakkonen, E. Ruoslahti, Nucleolin expressed at the cell surface is a marker of endothelial cells in angiogenic blood vessels, *J. Cell Biol.* 163 (2003) 871–878.
- [22] V. Moura, M. Lacerda, P. Figueiredo, M.L. Corvo, M.E. Cruz, R. Soares, M.C. de Lima, S. Simoes, J.N. Moreira, Targeted and intracellular triggered delivery of therapeutics to cancer cells and the tumor microenvironment: impact on the treatment of breast cancer, *Breast Can. Res. Treat* 133 (2012) 61–73.
- [23] H. Ginisty, H. Sicard, B. Roger, P. Bouvet, Structure and functions of nucleolin, *J. Cell Sci.* 112 (Pt 6) (1999) 761–772.
- [24] F. Mongelard, P. Bouvet, Nucleolin: a multiFACeTed protein, *Trends Cell Biol.* 17 (2007) 80–86.
- [25] H. Fujiki, T. Watanabe, M. Suganuma, Cell-surface nucleolin acts as a central mediator for carcinogenic, anti-carcinogenic, and disease-related ligands, *J. Can. Res. Clin. Oncol.* 140 (2014) 689–699.
- [26] D. Destouches, N. Page, Y. Hamma-Kourbali, V. Machi, O. Chaloin, S. Frechault, C. Birmapas, P. Katsoris, J. Beyrath, P. Albanese, M. Maurer, G. Carpentier, J. M. Strub, A. Van Dorsselaer, S. Muller, D. Bagnard, J.P. Briand, J. Courty, A simple approach to cancer therapy afforded by multivalent pseudopeptides that target cell-surface nucleoproteins, *Can. Res.* 71 (2011) 3296–3305.
- [27] D. Destouches, E. Huet, M. Sader, S. Frechault, G. Carpentier, F. Ayoul, J.P. Briand, S. Menashi, J. Courty, Multivalent pseudopeptides targeting cell surface nucleoproteins inhibit cancer cell invasion through tissue inhibitor of metalloproteinases 3 (TIMP-3) release, *J. Biol. Chem.* 287 (2012) 43685–43693.
- [28] P.J. Bates, D.A. Laber, D.M. Miller, S.D. Thomas, J.O. Trent, Discovery and development of the G-rich oligonucleotide AS1411 as a novel treatment for cancer, *Exp. Mol. Pathol.* 86 (2009) 151–164.
- [29] A.C. Gregorio, M. Lacerda, P. Figueiredo, S. Simoes, S. Dias, J.N. Moreira, Meeting the needs of breast cancer: a nucleolin's perspective, *Crit. Rev. Oncol. Hematol.* 125 (2018) 89–101.
- [30] Y.W. Eom, M.A. Kim, S.S. Park, M.J. Goo, H.J. Kwon, S. Sohn, W.H. Kim, G. Yoon, K.S. Choi, Two distinct modes of cell death induced by doxorubicin: apoptosis and cell death through mitotic catastrophe accompanied by senescence-like phenotype, *Oncogene* 24 (2005) 4765–4777.
- [31] S. Mansilla, W. Priebe, J. Portugal, Mitotic catastrophe results in cell death by caspase-dependent and caspase-independent mechanisms, *Cell Cycle* 5 (2006) 53–60.
- [32] A. Lucci, T.Y. Han, Y.Y. Liu, A.E. Giuliano, M.C. Cabot, Multidrug resistance modulators and doxorubicin synergize to elevate ceramide levels and elicit apoptosis in drug-resistant cancer cells, *Cancer* 86 (1999) 300–311.
- [33] Y.A. Hannun, L.M. Obeid, Sphingolipids and their metabolism in physiology and disease, *Nat. Rev. Mol. Cell Biol.* 19 (2018) 175–191.
- [34] Y.Y. Liu, T.Y. Han, A.E. Giuliano, M.C. Cabot, Expression of glucosylceramide synthase, converting ceramide to glucosylceramide, confers adriamycin resistance in human breast cancer cells, *J. Biol. Chem.* 274 (1999) 1140–1146.
- [35] Y.Y. Liu, V. Gupta, G.A. Patwardhan, K. Bhingre, Y. Zhao, J. Bao, H. Mehendae, M. C. Cabot, Y.T. Li, S.M. Jazwinski, Glucosylceramide synthase upregulates MDRI expression in the regulation of cancer drug resistance through cSrc and beta-catenin signaling, *Mol. Can.* 9 (2010) 145.
- [36] X. Su, H. Song, F. Niu, K. Yang, G. Kou, X. Wang, H. Chen, W. Li, S. Guo, J. Li, B. Li, S.S. Feng, J. Jiang, C. Yin, J. Gao, Co-delivery of doxorubicin and PEGylated C16-ceramide by nanoliposomes for enhanced therapy against multidrug resistance, *Nanomedicine (Lond)* 10 (2015) 2033–2050.
- [37] A. Overbye, A.M. Holsaeter, F. Markus, N. Skalko-Basnet, T.G. Iversen, M. L. Torgersen, T. Sonstevold, O. Engebraaten, K. Flatmark, G.M. Maelandsmo, T. Skotland, K. Sandvig, Ceramide-containing liposomes with doxorubicin: time and cell-dependent effect of C6 and C12 ceramide, *Oncotarget* 8 (2017) 76921–76934.
- [38] C. Ji, B. Yang, Y.L. Yang, S.H. He, D.S. Miao, L. He, Z.G. Bi, Exogenous cell-permeable C6 ceramide sensitizes multiple cancer cell lines to Doxorubicin-induced apoptosis by promoting AMPK activation and mTORC1 inhibition, *Oncogene* 29 (2010) 6557–6568.
- [39] X. Dong, C.A. Mattingly, M.T. Tseng, M.J. Cho, Y. Liu, V.R. Adams, R.J. Mumper, Doxorubicin and paclitaxel-loaded lipid-based nanoparticles overcome multidrug resistance by inhibiting P-glycoprotein and depleting ATP, *Can. Res.* 69 (2009) 3918–3926.
- [40] B.S. Zolnik, S.T. Stern, J.M. Kaiser, Y. Heakal, J.D. Clogston, M. Kester, S.E. McNeil, Rapid distribution of liposomal short-chain ceramide in vitro and in vivo, *Drug. Metab. Dispos.* 36 (2008) 1709–1715.
- [41] E. Khazanov, A. Prieve, J.P. Shilleman, Y. Barenholz, Physicochemical and biological characterization of ceramide-containing liposomes: paving the way to ceramide therapeutic application, *Langmuir* 24 (2008) 6965–6980.
- [42] S.A. Morad, M.C. Cabot, Ceramide-orchestrated signalling in cancer cells, *Nat. Rev. Can.* 13 (2013) 51–65.
- [43] T. Stover, M. Kester, Liposomal delivery enhances short-chain ceramide-induced apoptosis of breast cancer cells, *J. Pharmacol. Exp. Ther.* 307 (2003) 468–475.
- [44] S. Grosch, S. Schiffmann, G. Geisslinger, Chain length-specific properties of ceramides, *Prog. Lipid Res.* 51 (2012) 50–62.
- [45] A.F. Cruz, M.B. Caleiras, N.A. Fonseca, N. Goncalves, V.M. Mendes, S.F. Sampaio, V. Moura, J.B. Melo, R.D. Almeida, B. Manadas, S. Simoes, J.N. Moreira, The enhanced efficacy of intracellular delivery of doxorubicin/C6-ceramide combination mediated by the F3 peptide/nucleolin system is supported by the downregulation of the PI3K/Akt pathway, *Cancers (Basel)* 13 (2021).
- [46] K. Kitatani, T. Usui, S.K. Sriraman, M. Toyoshima, M. Ishibashi, S. Shigeta, S. Nagase, M. Sakamoto, H. Ogiso, T. Okazaki, Y.A. Hannun, V.P. Torchilin, N. Yaegashi, Ceramide limits phosphatidylinositol-3-kinase C2beta-controlled cell motility in ovarian cancer: potential of ceramide as a metastasis-suppressor lipid, *Oncogene* 35 (2016) 2801–2812.
- [47] J. Zhou, J. Wulfskuhle, H. Zhang, P. Gu, Y. Yang, J. Deng, J.B. Margolick, L. A. Liotta, E. Petricoin 3rd, Y. Zhang, Activation of the PTEN/mTOR/STAT3 pathway in breast cancer stem-like cells is required for viability and maintenance, *Proc. Natl. Acad. Sci. USA* 104 (2007) 16158–16163.
- [48] A. Dubrovka, S. Kim, R.J. Salamone, J.R. Walker, S.M. Maira, C. Garcia-Echeverria, P.G. Schultz, V.A. Reddy, The role of PTEN/Akt/PI3K signaling in the maintenance and viability of prostate cancer stem-like cell populations, *Proc. Natl. Acad. Sci. USA* 106 (2009) 268–273.
- [49] K. He, T. Xu, Y. Xu, A. Ring, M. Kahn, A. Goldkorn, Cancer cells acquire a drug resistant, highly tumorigenic, cancer stem-like phenotype through modulation of the PI3K/Akt/beta-catenin/CBP pathway, *Int. J. Can.* 134 (2014) 43–54.
- [50] T.C. Stover, A. Sharma, G.P. Robertson, M. Kester, Systemic delivery of liposomal short-chain ceramide limits solid tumor growth in murine models of breast adenocarcinoma, *Clin. Can. Res.: Off. J. Am. Assoc. Can. Res.* 11 (2005) 3465–3474.
- [51] H.R. Tagaram, N.A. Divittore, B.M. Barth, J.M. Kaiser, D. Avella, E.T. Kimchi, Y. Jiang, H.C. Isom, M. Kester, K.F. Staveley-O'Carroll, Nanoliposomal ceramide prevents in vivo growth of hepatocellular carcinoma, *Gut* 60 (2011) 695–701.
- [52] N.A. Fonseca, L.C. Gomes-da-Silva, V. Moura, S. Simoes, J.N. Moreira, Simultaneous active intracellular delivery of doxorubicin and C6-ceramide shifts the additive/antagonistic drug interaction of non-encapsulated combination, *J. Control Release* 196 (2014) 122–131.
- [53] E.M. Czekanska, Assessment of cell proliferation with resazurin-based fluorescent dye, *Methods Mol. Biol.* 740 (2011) 27–32.
- [54] T.C. Chou, Theoretical basis, experimental design, and computerized simulation of synergism and antagonism in drug combination studies, *Pharmacol. Rev.* 58 (2006) 621–681.
- [55] T.C. Chou, P. Talalay, Quantitative analysis of dose-effect relationships: the combined effects of multiple drugs or enzyme inhibitors, *Adv. Enzyme Regul.* 22 (1984) 27–55.
- [56] T.C. Chou, The mass-action law based algorithm for cost-effective approach for cancer drug discovery and development, *Am. J. Can. Res.* 1 (2011) 925–954.
- [57] A. Mateen, A.R. Adil, R.N. Maken, Q.A. Hashmi, F. Abdullah, A.M. Duraishi, Neoadjuvant cisplatin and doxorubicin in locally advanced triple negative breast cancer, *Journal of Clinical Oncology*, 34 (2016) e12511-e12511.
- [58] W. Ma, Q. Chen, W. Xu, M. Yu, Y. Yang, B. Zou, Y.S. Zhang, J. Ding, Z. Yu, Self-targeting visualizable hyaluronate nanogel for synchronized intracellular release of doxorubicin and cisplatin in combating multidrug-resistant breast cancer, *Nano Res.* 14 (2021) 846–857.
- [59] N.A. Fonseca, A.C. Gregório, V.M. Mendes, R. Lopes, T. Abreu, N. Goncalves, B. Manadas, M. Lacerda, P. Figueiredo, M. Pereira, M. Gaspar, F. Colelli, D. Pesce, G. Signorino, L. Focareta, A. Fucci, F. Cardile, C. Pisano, T. Cruz, L. Almeida, V. Moura, S. Simões, J.N. Moreira, GMP-grade nanoparticle targeted to nucleolin downregulates tumor molecular signature, blocking growth and invasion, at low systemic exposure, *Nano Today* 37 (2021), 101095.
- [60] I. Lopez-Montero, N. Rodriguez, S. Cribier, A. Pohl, M. Velez, P.F. Devaux, Rapid transbilayer movement of ceramides in phospholipid vesicles and in human erythrocytes, *J. Biol. Chem.* 280 (2005) 25811–25819.
- [61] J. Gasca, M.L. Flores, R. Jimenez-Guerrero, M.E. Saez, I. Barragan, M. Ruiz-Borrego, M. Tortolero, F. Romero, C. Saez, M.A. Japon, EDIL3 promotes epithelial-mesenchymal transition and paclitaxel resistance through its interaction with integrin alphaVbeta3 in cancer cells, *Cell Death Discov.* 6 (2020) 86.
- [62] A. Martowicz, G. Spizzo, G. Gastl, G. Untergasser, Phenotype-dependent effects of EpCAM expression on growth and invasion of human breast cancer cell lines, *BMC Can.* 12 (2012) 501.
- [63] D. Hanahan, R.A. Weinberg, Hallmarks of cancer: the next generation, *Cell* 144 (2011) 646–674.
- [64] H. Clevers, The cancer stem cell: premises, promises and challenges, *Nat. Med.* 17 (2011) 313–319.
- [65] B.B. Zhou, H. Zhang, M. Damelin, K.G. Geles, J.C. Grindley, P.B. Dirks, Tumour-initiating cells: challenges and opportunities for anticancer drug discovery, *Nat. Rev. Drug. Discov.* 8 (2009) 806–823.
- [66] X. Li, M.T. Lewis, J. Huang, C. Gutierrez, C.K. Osborne, M.F. Wu, S.G. Hilsenbeck, A. Pavlick, X. Zhang, G.C. Chamness, H. Wong, J. Rosen, J.C. Chang, Intrinsic resistance of tumorigenic breast cancer cells to chemotherapy, *J. Natl. Can. Inst.* 100 (2008) 672–679.
- [67] A.M. Calcagno, C.D. Salcido, J.P. Gillet, C.P. Wu, J.M. Fostel, M.D. Mumau, M. M. Gottesman, L. Varticovski, S.V. Ambudkar, Promoted drug selection of breast cancer cells and enrichment of cancer stem cell characteristics, *J. Natl. Can. Inst.* 102 (2010) 1637–1652.
- [68] C.J. Creighton, X. Li, M. Landis, J.M. Dixon, V.M. Neumeister, A. Sjolund, D. L. Rimm, H. Wong, A. Rodriguez, J.I. Herschkowitz, C. Fan, X. Zhang, X. He, A. Pavlick, M.C. Gutierrez, L. Renshaw, A.A. Larionov, D. Faratian, S. G. Hilsenbeck, C.M. Perou, M.T. Lewis, J.M. Rosen, J.C. Chang, Residual breast cancers after conventional therapy display mesenchymal as well as tumor-initiating features, *Proc. Natl. Acad. Sci. USA* 106 (2009) 13820–13825.
- [69] L.D. Mayer, T.O. Harasym, P.G. Tardi, N.L. Harasym, C.R. Shew, S.A. Johnstone, E. C. Ramsay, M.B. Bally, A.S. Janoff, Ratiometric dosing of anticancer drug

- combinations: controlling drug ratios after systemic administration regulates therapeutic activity in tumor-bearing mice, *Mol. Can. Ther.* 5 (2006) 1854–1863.
- [70] J.E. Lancet, G.L. Uy, J.E. Cortes, L.F. Newell, T.L. Lin, E.K. Ritchie, R.K. Stuart, S. A. Strickland, D. Hogge, S.R. Solomon, R.M. Stone, D.L. Bixby, J.E. Koltitz, G. J. Schiller, M.J. Wieduwilt, D.H. Ryan, A. Hoering, K. Banerjee, M. Chiarella, A. C. Louie, B.C. Medeiros, CPX-351 (cytarabine and daunorubicin) liposome for injection versus conventional cytarabine plus daunorubicin in older patients with newly diagnosed secondary acute myeloid leukemia, *J. Clin. Oncol.* 36 (2018) 2684–2692.
- [71] G.S. Laszlo, E.H. Estey, R.B. Walter, The past and future of CD33 as therapeutic target in acute myeloid leukemia, *Blood Rev.* 28 (2014) 143–153.
- [72] H. Herrmann, I. Sadovnik, G. Eisenwort, T. Rulicke, K. Blatt, S. Herndlhofer, M. Willmann, G. Stefanzl, S. Baumgartner, G. Greiner, A. Schulenburg, N. Mueller, W. Rabitsch, M. Bilban, G. Hoermann, B. Streubel, D.A. Vallera, W.R. Sperr, P. Valent, Delineation of target expression profiles in CD34+/CD38- and CD34+/CD38+ stem and progenitor cells in AML and CML, *Blood Adv.* 4 (2020) 5118–5132.
- [73] D. Ponti, A. Costa, N. Zaffaroni, G. Pratesi, G. Petrangolini, D. Coradini, S. Pilotti, M.A. Pierotti, M.G. Daidone, Isolation and in vitro propagation of tumorigenic breast cancer cells with stem/progenitor cell properties, *Can. Res.* 65 (2005) 5506–5511.
- [74] M. Cioce, S. Gherardi, G. Viglietto, S. Strano, G. Blandino, P. Muti, G. Ciliberto, Mammosphere-forming cells from breast cancer cell lines as a tool for the identification of CSC-like- and early progenitor-targeting drugs, *Cell Cycle* 9 (2010) 2878–2887.
- [75] N.A. Bourbon, L. Sandirasegarane, M. Kester, Ceramide-induced inhibition of Akt is mediated through protein kinase C $\zeta$ : implications for growth arrest, *J. Biol. Chem.* 277 (2002) 3286–3292.
- [76] S.A. Morad, J.C. Levin, S.S. Shanmugavelandy, M. Kester, G. Fabrias, C. Bedia, M. C. Cabot, Ceramide–antiestrogen nanoliposomal combinations–novel impact of hormonal therapy in hormone-insensitive breast cancer, *Mol. Can. Ther.* 11 (2012) 2352–2361.
- [77] N. Kramer, A. Walz, C. Unger, M. Rosner, G. Krupitza, M. Hengstschlager, H. Dolznig, In vitro cell migration and invasion assays, *Mutat. Res.* 752 (2013) 10–24.
- [78] S. Blockhuys, X. Zhang, P. Wittung-Stafshede, Single-cell tracking demonstrates copper chaperone Atox1 to be required for breast cancer cell migration, *Proc. Natl. Acad. Sci. USA* 117 (2020) 2014–2019.
- [79] S. Giampieri, C. Manning, S. Hooper, L. Jones, C.S. Hill, E. Sahai, Localized and reversible TGF $\beta$  signalling switches breast cancer cells from cohesive to single cell motility, *Nat. Cell Biol.* 11 (2009) 1287–1296.
- [80] A. Guerrero-Zotano, I.A. Mayer, C.L. Arteaga, PI3K/AKT/mTOR: role in breast cancer progression, drug resistance, and treatment, *Can. Metastasis Rev.* 35 (2016) 515–524.
- [81] E. Koedoot, M. Fokkelman, V.M. Rogkoti, M. Smid, I. van de Sandt, H. de Bont, C. Pont, J.E. Klip, S. Wink, M.A. Timmermans, E.A.C. Wiemer, P. Stoilov, J. A. Foekens, S.E. Le Devedec, J.W.M. Martens, B. van de Water, Uncovering the signaling landscape controlling breast cancer cell migration identifies novel metastasis driver genes, *Nat. Commun.* 10 (2019) 2983.